Article

Neuron

Reciprocal Activation within a Kinase-Effector Complex Underlying Persistence of Structural LTP

Highlights

- Persistent Rac1 activity is required for structural LTP of dendritic spines
- CaMKII stably binds on pseudo-autoinhibitory domain of Tiam1, a Rac-GEF
- This binding disinhibits autoinhibition of CaMKII and maintains its activity
- Persistently activated CaMKII phosphorylates Tiam1 and maintains Rac1 activity

Authors

Takeo Saneyoshi, Hitomi Matsuno, Akio Suzuki, ..., Margaret M. Stratton, Ryohei Yasuda, Yasunori Hayashi

Correspondence

saneyoshi.takeo.3v@kyoto-u.ac.jp (T.S.), yhayashi-tky@umin.ac.jp (Y.H.)

In Brief

Saneyoshi et al. find that stimulation of single spine causes rapid formation of a reciprocally activating signaling complex between CaMKII and a Rac-GEF Tiam1, which stably activates Rac1 and maintains enlarged spine structure during LTP.

Saneyoshi et al., 2019, Neuron *102*, 1–12
June 19, 2019
https://doi.org/10.1016/j.neuron.2019.04.012

CellPress

Please cite this article in press as: Saneyoshi et al., Reciprocal Activation within a Kinase-Effector Complex Underlying Persistence of Structural LTP, Neuron (2019), https://doi.org/10.1016/j.neuron.2019.04.012

Neuron
Article

Reciprocal Activation within a Kinase-Effector Complex Underlying Persistence of Structural LTP

Takeo Saneyoshi,[1,2,10,*] Hitomi Matsuno,[1] Akio Suzuki,[1] Hideji Murakoshi,[3,4,5] Nathan G. Hedrick,[4,5] Emily Agnello,[6,9] Rory O'Connell,[6] Margaret M. Stratton,[6] Ryohei Yasuda,[4] and Yasunori Hayashi[1,2,7,8,*]
[1]Brain Science Institute, RIKEN, Wako, Saitama 351-0198, Japan
[2]Department of Pharmacology, Kyoto University Graduate School of Medicine, Kyoto 606-8501, Japan
[3]National Institute of Physiological Science, Okazaki, Aichi 444-8585, Japan
[4]Max Planck Florida Institute for Neuroscience, Jupiter, FL 33458, USA
[5]Duke University Medical Center, Durham, NC 27703, USA
[6]Department of Biochemistry and Molecular Biology, University of Massachusetts, Amherst, MA 01003, USA
[7]Brain and Body System Science Institute, Saitama University, Saitama 338-8570, Japan
[8]School of Life Science, South China Normal University, Guangzhou 510631, China
[9]Present Address: Graduate school of Biomedical Sciences, University of Massachusetts, Worcester, MA 01655, USA
[10]Lead Contact
*Correspondence: saneyoshi.takeo.3v@kyoto-u.ac.jp (T.S.), yhayashi-tky@umin.ac.jp (Y.H.)
https://doi.org/10.1016/j.neuron.2019.04.012

SUMMARY

Long-term synaptic plasticity requires a mechanism that converts short Ca^{2+} pulses into persistent biochemical signaling to maintain changes in the synaptic structure and function. Here, we present a novel mechanism of a positive feedback loop, formed by a reciprocally activating kinase-effector complex (RAKEC) in dendritic spines, enabling the persistence and confinement of a molecular memory. We found that stimulation of a single spine causes the rapid formation of a RAKEC consisting of CaMKII and Tiam1, a Rac-GEF. This interaction is mediated by a pseudo-autoinhibitory domain on Tiam1, which is homologous to the CaMKII autoinhibitory domain itself. Therefore, Tiam1 binding results in constitutive CaMKII activation, which in turn persistently phosphorylates Tiam1. Phosphorylated Tiam1 promotes stable actin-polymerization through Rac1, thereby maintaining the structure of the spine during LTP. The RAKEC can store biochemical information in small subcellular compartments, thus potentially serving as a general mechanism for prolonged and compartmentalized signaling.

INTRODUCTION

Ever since long-term potentiation (LTP) of synaptic transmission was described in hippocampus (Nicoll, 2017, for review), the central question still remains: how is a persistent molecular memory generated from a transient modulation of neuronal activity? Ca^{2+}/calmodulin-dependent protein kinase II (CaMKII) has been proposed as a potential memory molecule because of its built-in self-activation mechanism. CaMKII is autophosphorylated at Thr 286 as a result of Ca^{2+} influx through the *N*-methyl-D-aspartic acid receptor (NMDAR), and as long as Thr 286 remains phosphorylated, CaMKII will remain in the "on" state, even in the absence of Ca^{2+} (Lisman et al., 2002; Hell, 2014). An *in vitro* reconstitution study indeed shows bistability of CaMKII (Urakubo et al., 2014), as predicted by the models (Zhabotinsky, 2000; Miller et al., 2005). However, recent imaging studies using a FRET sensor for CaMKII activity revealed that the bulk activity of CaMKII subsides within 1 min after the LTP-inducing stimulation (Takao et al., 2005; Lee et al., 2009). A photoactivatable CaMKII inhibitor paAIP2 is effective only when it is photoactivated during LTP induction but not during maintenance, which is also consistent with the imaging study (Murakoshi et al., 2017). On the other hand, the increase in AMPA-type glutamate receptor (AMPAR) transmission and structural enlargement of dendritic spine (structural LTP or sLTP) can be maintained for more than 1 h (Bosch and Hayashi, 2012; Nicoll, 2017). Thus, the mechanism that converts a transient Ca^{2+} signaling into persistent synaptic signaling during LTP has been a long-standing question.

One of the members of the Rho-family small G-protein, Rac1, is a major regulator of F-actin of particular interest in this context because modulation of its activity can alter the structure and function of excitatory synapses (Saneyoshi and Hayashi, 2012). Expression of a dominant-negative form of Rac1 or shRNA against Rac1 causes spine shrinkage and elimination, whereas a constitutively active form of Rac1 leads to an increase in spine density and clustering of AMPAR (Tashiro et al., 2000; Wiens et al., 2005). Knocking out Rac1 impairs LTP and spatial learning (Haditsch et al., 2009). One of the final effectors of Rac1 is cofilin, which rapidly and persistently (~1 h) accumulates in spines after LTP induction and regulates the dynamics of actin (Bosch et al., 2014; Noguchi et al., 2016). Indeed, a study monitoring local F-actin/G-actin equilibrium using FRET revealed that the equilibrium moves toward F-actin upon LTP induction for more than 30 min (Okamoto et al., 2004). This shift in F-actin/G-actin equilibrium increases the local amount of F-actin and contributes to an increase in dendritic spine size and enhances the binding capacity to other postsynaptic proteins. Therefore, we deemed

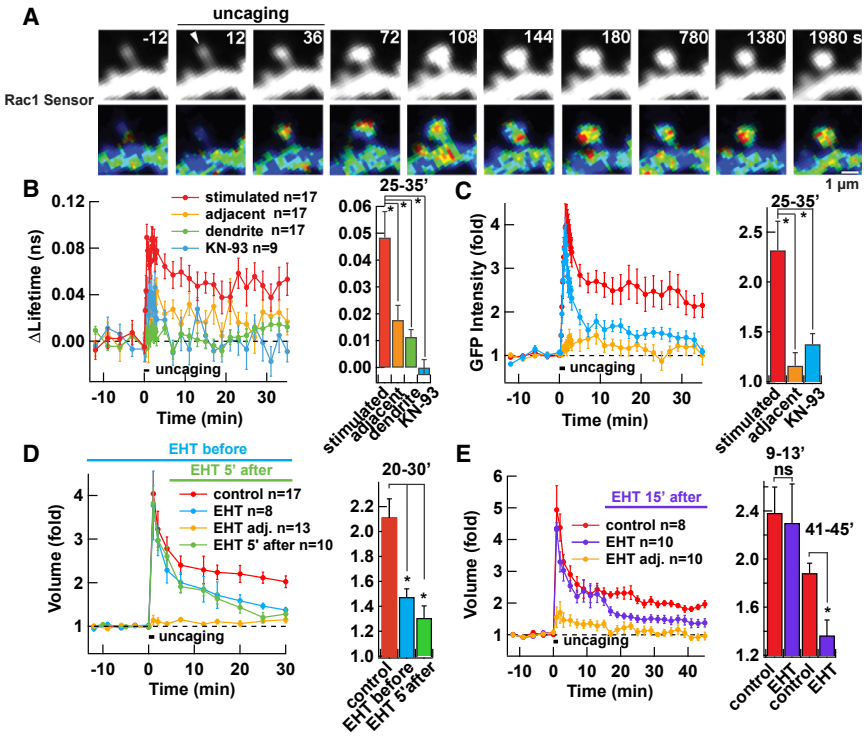

Figure 1. Persistent Rac1 Activation Is Required for sLTP in Hippocampal Organotypic Slice Culture

(A) Activation of Rac1, as visualized by FRET-FLIM-based Rac1 activity sensor during sLTP induced by uncaging caged glutamate at 0.5 Hz for 1 min. Rac1 activity and distribution of GFP-Rac1, as a proxy of structure, are shown. Warmer color hues in FLIM images indicate higher Rac1 activity. Arrowhead indicates the position of photo-uncaging.

(B) Averaged time course of Rac1 activation measured as a change in the lifetime of GFP-Rac1 from baseline in stimulated spines (stimulated, red), the dendritic shaft below the stimulated spines (dendrite, green), and adjacent spines (adjacent, yellow). Data from spines stimulated in the presence of CaMKII inhibitor KN-93 are also shown (blue). *$p < 0.05$, compared to stimulated spines; one-way ANOVA with the Dunnett's post hoc test comparisons.

(C) Averaged time course of GFP-Rac1 fluorescence intensity, measured as a proxy of volume change. *$p < 0.05$, compared to stimulated spines; one-way ANOVA with the Dunnett's post hoc test comparisons.

(D and E) Effect of Rac1 inhibitor EHT1864, applied 30 min before (blue) or 5 min after (green) (D), or 15 min after (purple) (E) induction of sLTP. Spines were visualized by expressing untagged GFP. *$p < 0.05$, compared to control; ns, not significant; one-way ANOVA with the Dunnett's post hoc test comparisons.

Data are represented as mean ± SEM in (B)–(E). See also Figure S1.

Rac1 to be a good candidate to mediate activity-dependent regulation of both the structure and function of excitatory synapses during LTP.

Rac1 is regulated by two major mechanisms (Saneyoshi and Hayashi, 2012). It is converted from an inactive GDP-bound form into an active GTP-bound form by guanine nucleotide exchange factors (GEFs) that stimulate the release of GDP to allow binding of GTP. GTP in the active form is hydrolyzed into GDP by their intrinsic GTPase activity, which is enhanced by GTPase-activating proteins (GAPs), resulting in inactivation of the G-proteins. In particular, RacGEFs such as Tiam1 and Kalirin-7/Trio are substrates of CaMKII and act as the site of action where neuronal activity regulates actin cytoskeleton during spine formation and development (Tolias et al., 2005; Xie et al., 2007; Penzes et al., 2008; Herring and Nicoll, 2016). Therefore, RacGEFs are ideally situated as a mediator of Ca^{2+} signaling to regulate synaptic structure and function.

In the present study, we probed the mechanism underlying the conversion from transient Ca^{2+} influx to persistent modulation of F-actin via the Rac1 signaling pathway. We propose a concept of a "reciprocally activating kinase-effector complex" (RAKEC). The influx of Ca^{2+} triggers the formation of a RAKEC between a "pseudo-autoinhibitory" domain on Tiam1 and a binding pocket "T-site" on CaMKII, normally occupied by the autoinhibitory domain of the kinase. Tiam1 binding interrupts autoinhibition of CaMKII resulting in its persistent activity, which, in turn, causes a persistent phosphorylation of Tiam1 and, therefore, an activation of Rac1 and downstream actin regulators. The RAKEC thus consists of a positive feedback loop, which enables the conversion of a transient Ca^{2+} signal triggered by the induction of LTP into a persistent kinase signal. RAKEC can store biochemical information in small subcellular compartments, thus potentially serving as a general mechanism for the production of prolonged and compartmentalized signaling.

RESULTS

Conversion Point of Temporary into Persistent Cellular Signal Is Located between CaMKII and Rac1

We monitored Rac1 activity in dendritic spines of CA1 pyramidal neurons in hippocampal organotypic slice cultures using a FRET-fluorescence lifetime imaging microscopy (FLIM) sensor composed of GFP-fused Rac1 and mCherry-fused Pak2-Rac1/Cdc42-binding domain (with R71C, S78A mutations) (Hedrick et al., 2016). Consistent with the previous study, upon induction of structural LTP (sLTP) using uncaging of glutamate on single spines, we observed an activation of Rac1 that lasted more than 30 min (Figures 1A–1C). The activation was significantly less in adjacent spines (average distance 2.7 ± 0.3 μm) and not observed in the dendritic shaft. The change in lifetime was not observed in neurons expressing GFP-Rac1 alone (not shown).

This prompted us to test the requirement of persistent activity of Rac1 in sLTP using a Rac inhibitor (EHT1864), which inhibits GTP loading of Rac (Shutes et al., 2007) (Figures 1D and 1E).

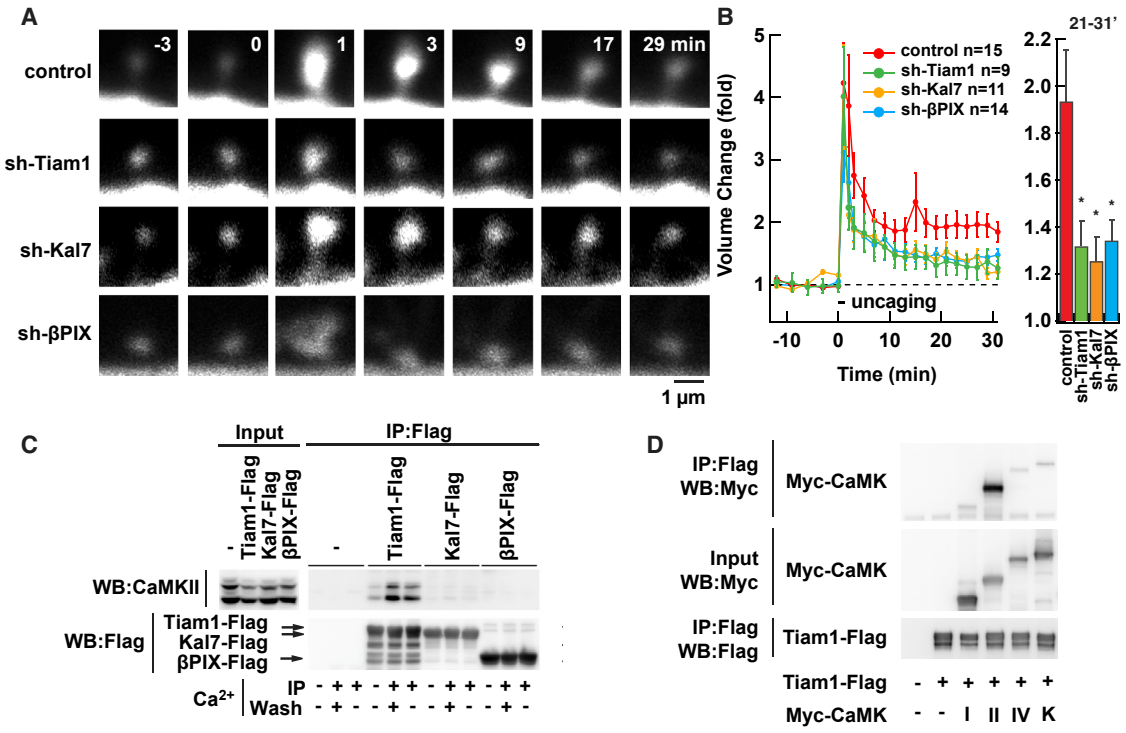

Figure 2. Ca^{2+}-Dependent Formation of a Stable Tiam1/CaMKII Complex

(A) Sample images of sLTP in neurons in hippocampal organotypic slice culture co-expressing GFP and shRNAs against luciferase (control), Tiam1, Kalirin-7 (Kal7), or βPIX.

(B) Summary of the effect of shRNAs. Spine volume was measured by fluorescent intensity of untagged GFP. *$p < 0.05$, compared to control; one-way ANOVA with the Dunnett's post hoc test comparisons. Data are represented as mean ± SEM.

(C) Persistent interaction between Tiam1 and CaMKII but not with Kalirin-7 and βPIX. The Flag-tagged RacGEF proteins were individually expressed in HEK293T cells. After lysing the cells, the RacGEFs were immunoprecipitated with Flag antibody and washed in the presence of Ca^{2+} (+) or absence (–, with EGTA). Endogenous CaMKII co-precipitated with RacGEF proteins were blotted against an anti-CaMKII antibody.

(D) A similar experiment with CaMK family kinases. CaMKIα, CaMKIIα, CaMKIV, and CaMKKα tagged with Myc epitope were co-expressed in HEK293T cells with Tiam1-Flag. CaMKs were co-immunoprecipitated with Flag-antibody in the presence of Ca^{2+} and detected with Myc antibody.

Representative blots were shown from at least three independent experiments in (C) and (D).

See also Figure S1.

Addition of this drug before sLTP induction effectively inhibited sLTP. When we added the drug either 5 or 15 min after the induction of sLTP, we found that it also effectively blocked sLTP, once established. These results indicate that the persistent activation of Rac1 by RacGEFs is indeed required for the maintenance of sLTP.

In order to examine the upstream signaling of the Rac1 activation, we used KN-93, an inhibitor of CaMKII that prevents the interaction of CaMKII with Ca^{2+}/calmodulin (Figures 1B and 1C). KN-93 also effectively blocked the activation of Rac1, indicating that Rac1 is downstream to CaMKII. Given that the activation of CaMKII returns to baseline levels within 1 min (Figures S1A–S1C), as revealed by CaMKII FRET sensor Camui (Takao et al., 2005; Lee et al., 2009), the conversion of transient signal into persistent signal must occur between Rac1 and CaMKII.

Activation of CaMKII Induces Association with RacGEF Tiam1

GEFs are major players in the process of small G-protein activation. Certain RacGEFs, such as Tiam1, Kalirin-7/Trio, and βPIX, have been shown to be downstream of the NMDAR and CaMK signaling (Fleming et al., 1999; Tolias et al., 2005; Xie et al., 2007; Saneyoshi et al., 2008; Herring and Nicoll, 2016). Thus, we tested involvement of these RacGEFs in sLTP by using specific shRNAs. All of these shRNAs reduced sLTP, though none of them completely abolished it (Figures 2A and 2B; $p < 0.05$ for all shRNAs compared with luciferase shRNA). The efficacy of these three shRNAs was comparable as assessed by immunostaining (Figures S1D and S1E).

Interestingly, there was one difference among the three RacGEFs tested. When we compared the interaction between CaMKII and RacGEFs by co-immunoprecipitation, we found only Tiam1 formed a stable complex with CaMKII (Figure 2C). Formation of this complex depends on the presence of Ca^{2+}. Furthermore, once formed, the complex remained intact even when EGTA was used to chelate the Ca^{2+}. In contrast, Kalirin-7 and βPIX did not form stable complexes that could be detected by co-immunoprecipitation. Other members of the CaMK family did not show such complex formation (Figure 2D), indicating the specificity of this interaction. We also confirmed the interaction

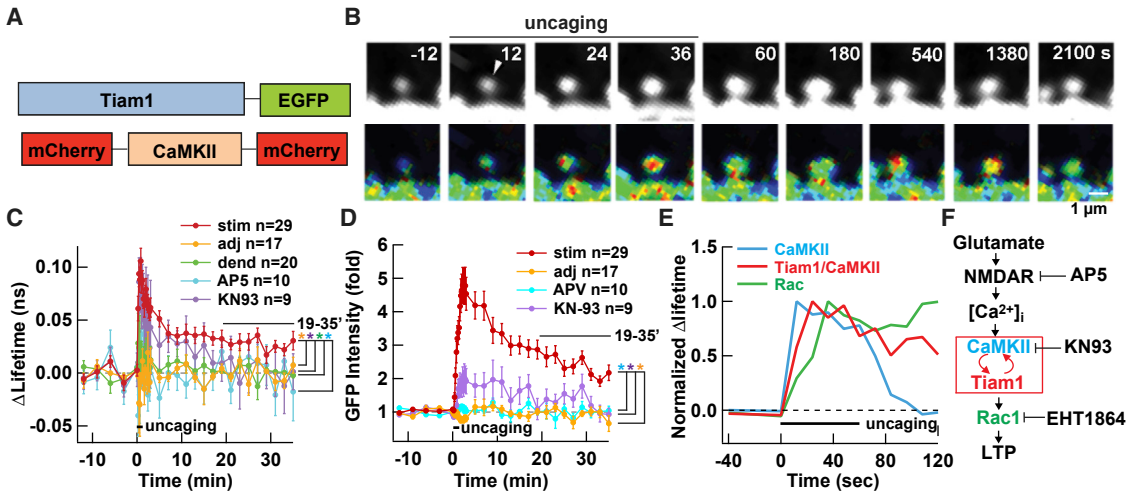

Figure 3. The Tiam1/CaMKII Interaction Is Persistent after sLTP Induction in Hippocampal Organotypic Slice Culture

(A) FRET-FLIM probe used to detect the interaction between Tiam1 and CaMKII.

(B) Interaction between Tiam1 and CaMKII as visualized by FRET-FLIM before and during sLTP (top). Warmer hues indicate more interaction. The distribution of Tiam1-GFP, as a proxy of structure, is shown (bottom).

(C and D) Summary of Tiam1/CaMKII interaction (C) and volume of the spine as measured by Tiam1-GFP fluorescent intensity (D). *$p < 0.05$, compared to the stimulated spines; one-way ANOVA with the Dunnett's post hoc test comparisons. Data are represented as mean ± SEM.

(E) Comparison of the time course of CaMKII activation (Figure S1), Tiam1/CaMKII interaction, and Rac1 activation (Figure 1). The graphs are normalized by the largest value of lifetime change.

(F) Schematic of the signaling cascade leading to LTP. T-shaped bar indicates inhibition. Red arrows indicate positive feedback loop.

See also Figure S2.

between endogenous Tiam1 and CaMKII in brain by co-immunoprecipitation (Figure S2A).

Then, we investigated whether Tiam1 and CaMKII interact with each other in a single spine by sLTP induction by measuring FRET between a donor Tiam1-GFP and an acceptor mCherry-CaMKII-mCherry fusion protein using FLIM (Figure 3A). Following the induction, there was a rapid increase in FRET in the stimulated spine, indicating that these two proteins interact with each other after LTP induction (Figures 3B–3D). The increase in interaction partially subsided after 10 min but a fraction persisted for more than 30 min. This is a stark contrast with the activation time course of CaMKII FRET sensor, Camui, which returns to the baseline within 1 min (Takao et al., 2005; Lee et al., 2009) (Figures S1A–S1C). Importantly, the interaction between Tiam1 and CaMKII was blocked by bath application of NMDAR antagonist (AP5), KN-93, and cotransfection of endogenous CaMKII inhibitor protein (CaMKIIN) (Figures 3C, 3D, and S2B–S2D). These results indicate that the complex between Tiam1 and CaMKII is dependent on the influx of Ca^{2+} through the NMDAR and subsequent activation of CaMKII. By plotting the time course of activation, it is clear that the bulk of CaMKII is activated first, followed by the interaction between CaMKII and Tiam1, and finally Rac1 activation (Figure 3E). This order of activation corroborates the biochemical cascade, indicating causality (Figure 3F). It should be noted, however, that we do not rule out the possibility that two other RacGEFs, Kalirin-7 and βPIX, are also involved in sLTP. They are indeed both situated downstream of CaMK signaling pathway and involved in activity-dependent spine morphogenesis and plasticity (Xie et al., 2007; Saneyoshi et al., 2008; Herring and Nicoll, 2016). Whether these molecules are involved in the maintenance phase of sLTP and if they do, how their signaling is maintained will be of particular interest.

Tiam1 Competes with the Autoinhibitory Domain of CaMKII for T-Site

Then, we used Tiam1-deletion mutants to map the interaction region (Figures 4A and 4B). We identified the region containing residues 1,540–1,591 at the carboxyl tail, a region without a known function, to be important for this interaction. Alanine scanning of three consecutive residues at a time further narrowed down the binding region to residues 1,543–1,557 (Figure 4C). The sequence around this region is well conserved across vertebrate species (Figure S3A). In order to obtain quantitative information on the interaction, we performed a fluorescence polarization assay with a fluorescently labeled Tiam1 peptide (residues 1,540–1,560) and the purified kinase domain of CaMKIIα (residues 6–274 with a kinase null D135N mutation). We found that the peptide and CaMKII directly interact with a K_D of 8.1 ± 1.7 μM, which could be competed off with an excess amount of unlabeled peptide (Figure 4E). Free fluorescein did not show specific binding (Figure 4D).

Upon inspection of the sequence of Tiam1 involved in CaMKII binding, we noticed that it has homology with the autoinhibitory domain of CaMKII, which normally prevents substrate binding by docking on a region called the "T-site" that is adjacent to the substrate-binding "S-site" (Figure 4F) (Lisman et al., 2002). Given the homology, we wondered whether Tiam1 interacts with CaMKII at the T-site. To test this, we used several peptides

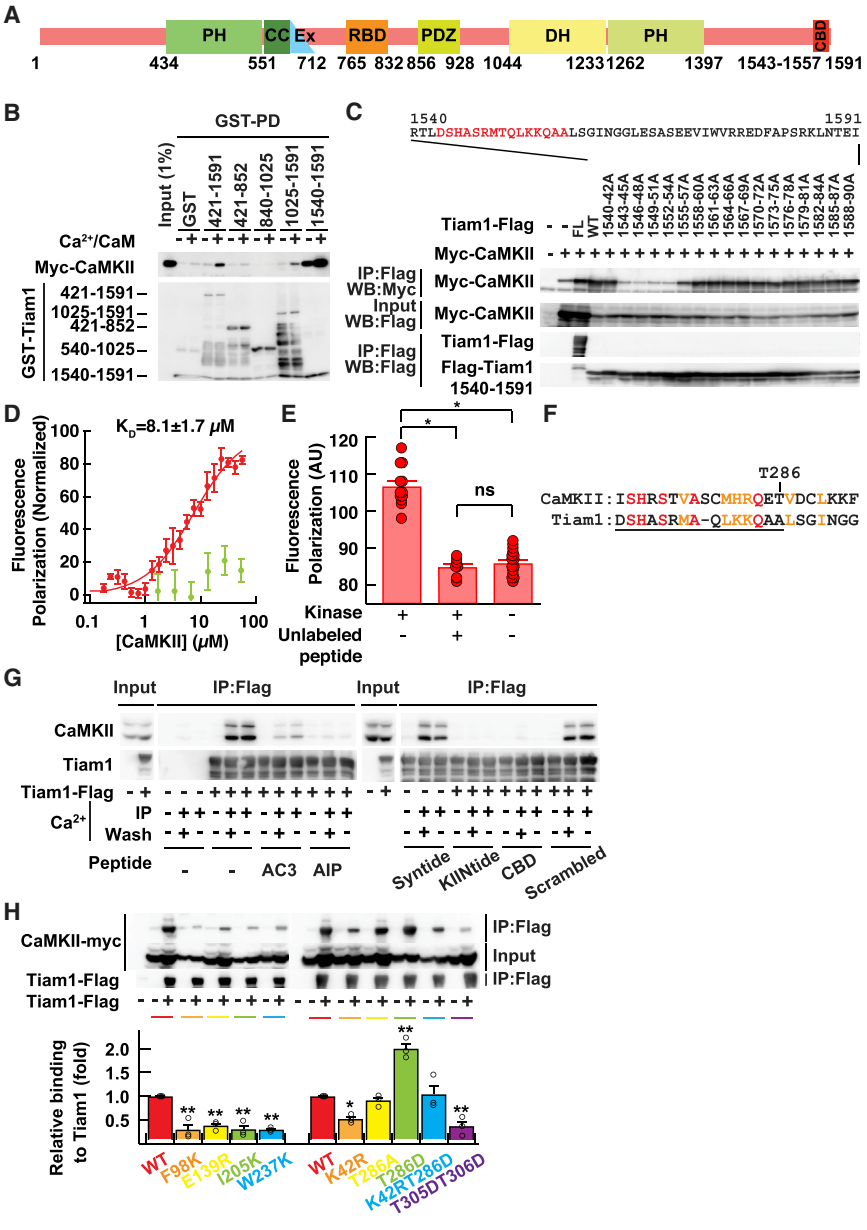

Figure 4. Tiam1 Interacts with CaMKII T-Site

(A) Domain structure of Tiam1. The identified CaMKII-binding domain (CBD) is located at the carboxyl tail of Tiam1. PH, pleckstrin-homology domain; CC, coiled-coil region; Ex, extra domain; RBD, Ras-binding domain; PDZ, PSD-95/Dlg/ZO1 domain; and DH, Dbl-homology domain.

(B) Mapping of the binding domain of Tiam1 by GST-pull-down (PD) assay. Myc-tagged CaMKII expressed in HEK293T cells were incubated with immobilized Tiam1 fragments in the presence or absence of Ca^{2+}. Bound CaMKII was detected by western blotting with Myc antibody. Bars at the left side of bottom image show expected positions of the each Tiam1 fragment fused with GST except 1,540–1,591, which runs at the dye front.

(C) Identification of CaMKII-binding region in Tiam1 by alanine scanning. Full-length Tiam1 (FL), 1,540–1,591 fragment of either WT sequence or alanine mutants introduced in three consecutive residues were co-expressed with Myc-CaMKII in HEK293T cells. Cell lysates were immunoprecipitated with a Flag antibody in the presence of Ca^{2+}. Immunoprecipitated proteins were detected by western blot using Myc and Flag antibodies.

(D) Estimate of the binding affinity by fluorescence polarization. Fluorescein-labeled Tiam1 peptide corresponding to residues 1,540–1,560 (red) and bacterially expressed kinase domain of CaMKII 6-274 with kinase null D135N mutation were used. Fluorescein (green) was used as negative control. n = 6 for peptide and 3 for fluorescein.

(E) Fluorescence-polarization assay with competing unlabeled peptide. The assay was the same as (D) except for the addition of unlabeled Tiam1 peptide (50 μM). Kinase was at 10 μM. n = 12 for CaMKII/Fluorescein-labeled Tiam1 peptide; n = 7 for CaMKII/Fluorescein-labeled Tiam1 peptide/unlabeled peptide; n = 16 for fluorescein-labeled Tiam1 peptide. *, $\alpha = 0.001$; ns, not significant; one-way ANOVA followed by the Tukey's HSD post hoc test.

(F) Similarity between autoinhibitory domain of CaMKII (CaMK2A, residue number, 271–293; GenBank: NM_171825) and the CaMKII-binding domain of Tiam1 (1,544–1,565; GenBank: NM_003253.2). Identical amino acids are shown in red and conservative residues were in orange. CBD is underlined.

(G) Competition of Tiam1/CaMKII interaction by peptides known to bind either the S- or T-site of CaMKII. HEK293T cells were transfected with Flag-tagged Tiam1. Cell lysates were immunoprecipitated with Flag antibody in the presence of Ca^{2+} (+) or EGTA (−) with or without the peptide inhibitors (5 μM). AC3, autocamtide 3; AIP, autocamtide-2-related inhibitory peptide; KIINtide, CaMKIINtide; and Scrambled, scrambled CBD. After washing, samples were eluted with SDS-PAGE sample buffer and immunoblotted with CaMKII and Flag antibodies.

(H) Effects of T-site (F98K, E139R, I205K, or W237K), kinase null (K42R), autophosphorylation deficient and mimic (T286A and T286D, respectively), and Ca^{2+}/calmodulin-binding deficient (T305D/T306D) mutations in CaMKII on interaction with Tiam1. The amount of immunoprecipitated CaMKII mutants was normalized by the total amount of the respective mutant. *$p < 0.05$, **, < 0.01, compared to WT CaMKII; one-way ANOVA with the Dunnett's post hoc test comparisons. Representative blots were shown from at least three independent experiments in (B), (C), and (F). Data are represented as mean ± SEM in (D), (E), and (H). See also Figure S3.

known to bind either S- or T-sites in order to compete with the Tiam1/CaMKII interaction (Figure 4G). Syntide 2, an S-site-binding peptide, did not interfere with the Tiam1/CaMKII interaction. In contrast, autocamtide-3 (AC3) and autocamtide 2-related inhibitory peptide (AIP), which mimic the autoinhibitory domain of CaMKII (Ishida and Fujisawa, 1995), and CaMKIIN, which is known to interact with the T-site (Vest et al., 2007), effectively blocked the Tiam1/CaMKII interaction. This indicates that Tiam1 interacts with CaMKII at the T-site in a manner competing with the autoinhibitory domain.

To gain more molecular insight, we modeled the Tiam1/CaMKII interaction using the crystal structure of CaMKIIN bound

to CaMKII as a starting point (Figures S3B–S3F) (Chao et al., 2010) and performed an energy minimization of the Tiam1 peptide. The resultant model shows that the basic residues (H1545, R1548, and K1554) interact with acidic residues on CaMKII. Also, hydrophobic residues (L1552 and L1558) fit into hydrophobic grooves in the kinase. These residues, which appear to be critical for binding, are largely consistent with the results from alanine scanning of CaMKIIN (Coultrap and Bayer, 2011). Consistent with this model, mutations in the T-site of CaMKII (F98K, E139R, I205K, and W237K) (Figure 4H) abolished the interaction with Tiam1.

We also carried out an additional mutagenesis to test how the interaction with Tiam1 is regulated (Figure 4H). A CaMKII mutant deficient in Ca^{2+}/calmodulin binding (T305D/T306D) and one deficient in kinase activity (K42R) both showed diminished binding to Tiam1. A constitutively active CaMKII mutant (T286D) showed increased binding whereas an autophosphorylation deficient mutant (T286A) and a double mutant (K42R/T286D) showed binding comparable to wild-type (WT). The reduced binding in the T305D/T306D mutant confirmed that the T-site first must be exposed by Ca^{2+}/calmodulin binding before Tiam1 can interact with CaMKII at the T-site. The enhanced binding in the T286D mutant indicates that an autophosphorylation at T286 facilitates Tiam1 binding. However, the observation that the T286A mutant showed comparable binding indicates T286 phosphorylation is not an absolute requirement. The observation that the catalytically inactive mutant (K42R) showed diminished binding suggests that there may be CaMKII phosphorylation sites on Tiam1 and/or nucleotide binding to CaMKII that facilitate binding (Coultrap and Bayer, 2011). In the K42R/T286D mutant, the effect of T286D was canceled out by the K42R mutation and thus showed intermediate binding.

Reciprocal Activation of CaMKII and Tiam1 in the Complex

If Tiam1 competes with the autoinhibitory domain of CaMKII for the same T-site, the binding may modulate the activity of the kinase. To test the activity of CaMKII complexed with Tiam1, purified WT or T286A mutant CaMKII was mixed with a GST-Tiam1 1,540–1,591 fragment in the presence of Ca^{2+}/calmodulin. ATP was omitted at this step to avoid inducing CaMKII autophosphorylation. Subsequently, Ca^{2+} was chelated using EGTA, ATP was added, and then the constitutive kinase activity was measured using Homer3 as a substrate (Figure 5A, left) (Bayer et al., 2006; Kim et al., 2015). CaMKII without Tiam1 (GST only) did not show any activity. However, when complexed to Tiam1, CaMKII exhibited pronounced kinase activity leading to Homer3 phosphorylation. Importantly, this activity was independent of T286 autophosphorylation because the T286 phosphorylation was not detected under this condition as revealed by blotting with pT286 antibody. Also, the activity of Tiam1-bound T286A CaMKII mutant was comparable to WT in the presence of EGTA. In the presence of Ca^{2+}/calmodulin, Homer3 was phosphorylated at a similar level under these conditions, indicating that each reaction has a comparable level of the enzyme (Figure 5A, right). The interaction with purified full-length Tiam1 also induced Ca^{2+}/calmodulin-independent activity of CaMKII (Figure S4A). These results confirm that once the complex between Tiam1 and the T-site of CaMKII has formed, CaMKII maintains activity, even in the absence of Ca^{2+}/calmodulin in a T286 phosphorylation independent manner. The T-site-binding region of Tiam1 works as a pseudo-autoinhibitory domain to dislodge the autoinhibitory domain of CaMKII and, instead of inhibiting, maintains CaMKII in its active conformation.

Finally, we confirmed that phosphorylation of Tiam1 by CaMKII activates its RacGEF activity by a pull-down assay with the Pak1-p21-binding domain, which preferentially binds to active Rac1/Cdc42 (Figure 5B). Indeed, Tiam1 phosphorylation by CaMKII significantly increased RacGEF activity, consistent with a previous study (Fleming et al., 1999). In sum, these two proteins form a reciprocally activating kinase-effector complex (RAKEC); Ca^{2+}-dependent Tiam1 binding to T-site of CaMKII via its pseudo-autoinhibitory domain induces Ca^{2+}-independent kinase activity, which, in turn, maintains Tiam1 phosphorylation and its RacGEF activity.

RAKEC Formed between Tiam1 and CaMKII Maintains RacGEF Activity after Chemical LTP Induction by Persistent Phosphorylation

Next, we tested whether binding of Tiam1 with CaMKII contributes to the regulation of Tiam1 RacGEF activity in neurons. We induced chemical LTP in hippocampal dissociated culture preparations, which has been shown to increase AMPAR transmission as well as the volume of dendritic spines (Bosch et al., 2014). We found Tiam1 RacGEF activity was persistently increased after chemical LTP induction with 200 μM glycine for 10 min by using a Rac1 G15A pull-down assay, which preferentially isolates activated RacGEFs (Figure 5C) (García-Mata et al., 2006; Um et al., 2014). We then monitored Tiam1 phosphorylation under these conditions using Phos-tag SDS-PAGE, which allows separation of phosphorylated protein (slower migration) from unphosphorylated proteins (faster migration) on the gel (Figure 5D). When phosphorylated Tiam1 samples were treated with λ phosphatase, the slowly migrating population was diminished, confirming that this population was indeed phosphorylated. Chemical LTP induction in the culture resulted in a persistent increase in the slowly migrating component, which was observed as a smeary pattern on the Phos-tag SDS-PAGE. This was blocked by CaMKII inhibitor KN-93 (Figure 5E), which indicates that multiple sites on Tiam1 are phosphorylated by CaMKII. To test the contribution of the RAKEC formed between Tiam1 and CaMKII on Tiam1 phosphorylation in neurons, we created a Tiam1 mutant where three residues, 1,552–1,554 (LKK), were replaced by alanine (Tiam1-AAA) to render it unable to bind CaMKII (Figure 4C). The mutant showed a significant reduction in phosphorylation even though all phosphorylation sites were intact, indicating that the RAKEC formed between Tiam1 and CaMKII is required to maintain the phosphorylated state of Tiam1 (Figure 5F). These results indicate that chemical induction of LTP induces the persistent phosphorylation of Tiam1 through the CaMKII/Tiam1 RAKEC even after the Ca^{2+} signal dissipates.

RAKEC Formed between Tiam1 and CaMKII Is Required for sLTP

We were curious whether the RAKEC formed between the Tiam1 carboxyl tail and CaMKII T-site is necessary for sLTP. For this

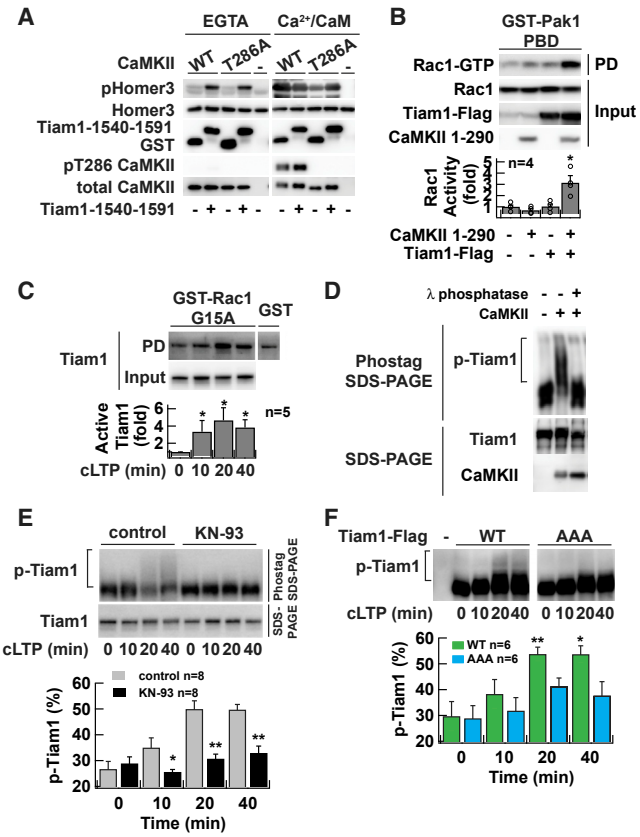

Figure 5. RAKEC Formation between CaMKII and Tiam1 Is Required for Tiam1 Phosphorylation during LTP

(A) *In vitro* kinase assay of Tiam1-bound CaMKII. CaMKII was affinity-purified with a Flag antibody from HEK293T cells expressing Flag-tagged CaMKII and incubated with GST-Tiam1 fragment (residue 1,540–1,591) or GST in the presence of Ca^{2+}/calmodulin to form a complex. Then EGTA was added to chelate Ca^{2+}. ATP was omitted in these steps to avoid autophosphorylation. *In vitro* phosphorylation reaction was carried out in the absence (EGTA) or presence of Ca^{2+}/calmodulin (Ca^{2+}/CaM) using purified GST-Homer3 as a substrate after adding ATP. The reaction products were subjected to western blotting with antibodies against phosphorylated-Homer3 (pHomer3) (Mizutani et al., 2008), GST, T286 phosphorylated CaMKII (pT286 CaMKII), and CaMKII.

(B) Activation of Tiam1 by CaMKII. Tiam1 was co-expressed with a constitutively active form of CaMKII (1–290) in HEK293T cells. Activated Rac1 was pulled down with Pak1-p21-binding domain, which specifically binds to the GTP-bound form of Rac1. *$p < 0.05$, compared to non-transfected cells; t test.

(C) Persistent activation of Tiam1 RacGEF after chemical LTP induction in neurons in dissociated culture demonstrated by Rac1-G15A pull-down assay. Activated Tiam1 in the lysate of neurons underwent glycine stimulation and were subject to a pull-down assay using a nucleotide-free Rac1 G15A mutant, which selectively binds to activated RacGEFs. Bound Tiam1 was detected by western blotting with anti-Tiam1 antibody. *$p < 0.05$, compared to non-stimulated neurons; Wilcoxon signed-rank test.

(D) Phos-tag SDS-PAGE analysis of Tiam1 protein. Tiam1-Flag proteins were purified from transfected HEK293T cells with Flag-agarose and incubated with Mg^{2+}/ATP, and 20 nM of CaMKII. The samples were treated with 10 U of λ phosphatase for 60 min at 30°C. Samples were resolved either 7.5-μM Phos-tag SDS-PAGE (top) or conventional SDS-PAGE (bottom). Tiam1 and CaMKII proteins were detected by western blotting with anti-Tiam1 or CaMKII antibodies, respectively. Slowly migrating species represent phosphorylated proteins. The reason why shifted band does not form a discrete ladder is likely because of the existence of multiple phosphorylation sites on Tiam1.

(E) Persistent phosphorylation of Tiam1 after chemical LTP induction in neurons in dissociated culture. Lysate from neurons that underwent chemical LTP induction with glycine for 10 min in the absence or presence of CaMKII inhibitor KN-93 (10 μM) were subject to Phos-tag SDS-PAGE to separate phosphorylated protein from unphosphorylated protein on a gel and then blotted with anti-Tiam1 antibody. Lower blot is a conventional SDS-PAGE. *$p < 0.05$, **$p < 0.01$, compared to control; one-way ANOVA followed by the Tukey's HSD post hoc test.

(F) The persistent phosphorylation requires Tiam1/CaMKII complex formation. Flag-tagged Tiam1 (WT or AAA mutant) was introduced into neurons in dissociated culture using a lentiviral vector. Phosphorylated Tiam1 was detected similarly to (E). except that anti-Flag antibody was used. *$p < 0.05$, **$p < 0.01$, compared to non-stimulated WT; one-way ANOVA with the Dunnett's post hoc test comparisons.

Representative blots are shown from at least three independent experiments in (A) and (D). Data are represented as mean ± SEM in (B), (C), (E), and (F). See also Figure S4.

purpose, we overexpressed a GFP-tagged Tiam1 WT or AAA mutant in neurons in slice culture and monitored sLTP as above to start. At the same time, we monitored Tiam1/CaMKII interaction by FRET-FLIM with mCherry-CaMKII-mCherry while measuring the volume change by using Tiam1-GFP fluorescence intensity as a proxy. We confirmed that CaMKII and Tiam1-AAA did not interact in this assay (Figures 6A–6D). Concomitantly, sLTP was severely diminished compared to the neurons expressing WT Tiam1. This indicates that the interaction between the carboxyl tail of Tiam1 and CaMKII is important for sLTP.

Then, we tested whether the persistent activation of Rac1 observed during sLTP actually requires the RAKEC formation between Tiam1 and CaMKII. We monitored Rac1 activity by FRET-FLIM in the presence of the Tiam1-AAA mutant to abolish complex formation while downregulating endogenous Tiam1 with shRNA. The rescue constructs of both Tiam1 WT and AAA were expressed at a comparable level in neurons in slice culture (Figures S4B and S4C). We found that Rac1 activation and sLTP were both significantly impaired (Figure 6E). These results confirm that the RAKEC formed between Tiam1 and CaMKII is indeed required for persistent Rac1 activation and underlies sLTP.

A study using photoactivatable CaMKII-inhibitor AIP (paAIP2) reported that photoactivation of paAIP2 failed to reverse established sLTP, although it is effective in blocking sLTP if activated during the induction (Murakoshi et al., 2017). Therefore, it was concluded that there is no contribution of CaMKII activity in sLTP maintenance, which is seemingly contradictory to current results. CaMKII-inhibitor peptide AIP and Tiam1 both interact with the T-site of CaMKII (Ishida and Fujisawa, 1995). Therefore, we hypothesized that Ca^{2+}/calmodulin-activated versus Tiam1-activated CaMKII may have different sensitivities to AIP. To test this possibility, we monitored Tiam1/CaMKII interaction by FRET while we activated paAIP2. As a result, we found that Tiam1/CaMKII interaction was insensitive to paAIP2 (Figure S5). In separate experiments, we confirmed that the activation of paAIP2 during glutamate uncaging did block sLTP (Figures S5A and S5B). This indicates that the experiment using paAIP2 cannot rule out the possibility of persistent activation of CaMKII through a mechanism mediated by T-site. When the CaMKII T-site is already occupied by Tiam1, AIP needs to

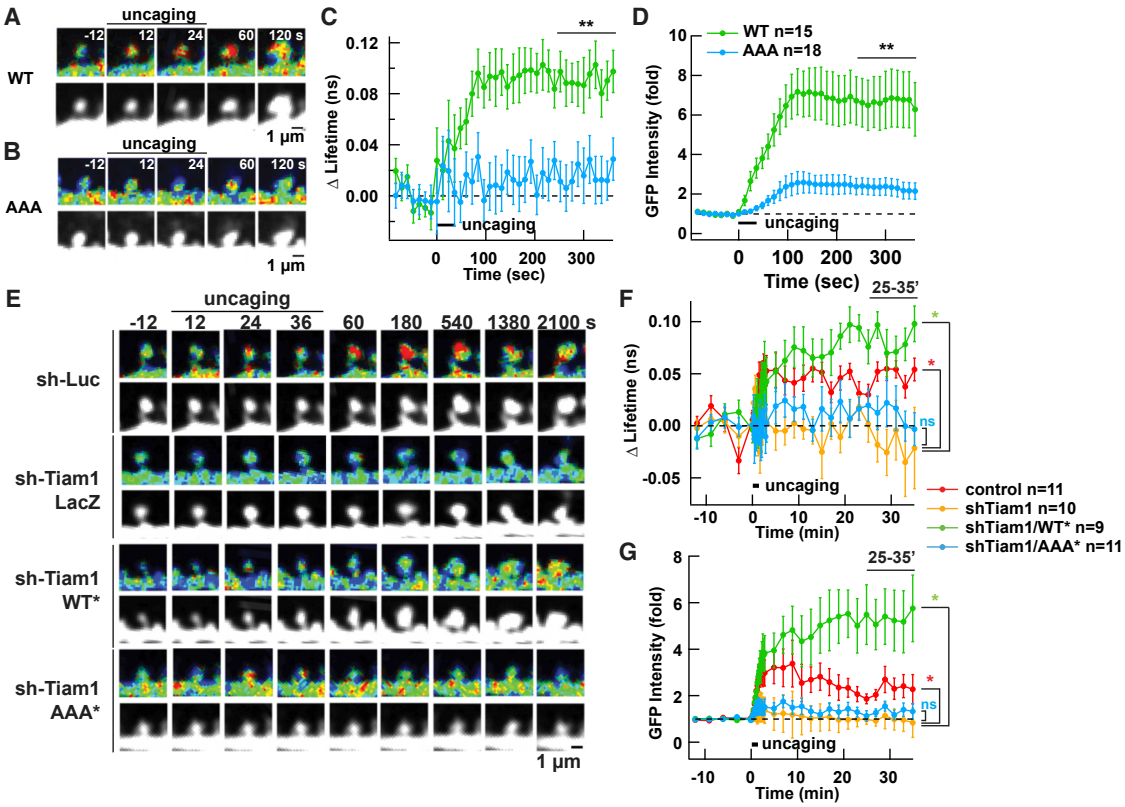

Figure 6. RAKEC Formation between Tiam1 and CaMKII Is Required for Persistence of sLTP and Rac1 Activity in Hippocampal Organotypic Slice Culture

(A and B) Interaction of Tiam1 with CaMKII T-site is required for sLTP. Interaction between Tiam1 WT (A) or AAA mutant (B, residues 1,552–1,554 were replaced by alanine) and CaMKII were measured using a FRET-FLIM sensor for Tiam1/CaMKII interaction similarly to Figure 1 but by using slice kept in culture for 2 weeks. Only the early phase of sLTP was tested.

(C and D) Summary of FRET change (C) and volume (D, using amount of Tiam1-GFP as a proxy of structure, as opposed to Figures 1D and 1E, where free GFP was used) from multiple spines. **$p < 0.01$, compared to WT and AAA; t test.

(E) Activation of Rac1 as visualized by FRET-FLIM-based Rac1 activity sensor during sLTP in neurons co-expressing shRNA against Tiam1, without or with Tiam1 rescue constructs. of either WT or AAA mutant.

(F and G) Averaged time course of Rac1 activation (F) and GFP-Rac1 fluorescent intensity change (G). Other conventions are similar to Figure 1. *$p < 0.05$, compared to parenthesized pair; n.s., not significant; one-way ANOVA followed by the Tukey's HSD post hoc test.

Data are represented as mean ± SEM in (C), (D), (F), and (G).

See also Figures S4 and S5.

compete it off in order to bind. It is likely that this reduces the potency of AIP and explains the inability of paAIP2 to block LTP during maintenance phase.

DISCUSSION

The mechanism of forming a persistent molecular memory from a transient Ca^{2+} signal has been a long-standing mystery. Here, we aimed to elucidate this mechanism and as a result we investigated the signaling pathways that lead to actin remodeling in the dendritic spine.

A Synaptic Ca^{2+} Signal Is Converted into RAKEC Formation

We identified a novel cellular mechanism, RAKEC, which controls the spatiotemporal pattern of a specific kinase signaling mechanism (Figure 7). We propose that the binding of a kinase to a class of effectors that harbor a specific sequence homologous to the autoinhibitory domain of the kinase (here termed pseudo-autoinhibitory domain) displaces the autoinhibitory domain to relieve the kinase from autoinhibition. Consequently, the activated kinase maintains the phosphorylated state of the effector. This creates a reciprocally activating positive feedback loop between the effector and the kinase, which significantly prolongs the duration of downstream cellular signaling. We demonstrated that the RacGEF Tiam1 maintains activity of CaMKII as well as its own phosphorylation status through this mechanism even after intracellular Ca^{2+} has diminished. This maintains Rac1 activity, F-actin organization, and, eventually, the enlarged spine structure. This is the first experimentally identified positive feedback loop with an inherent bistability defined by bound/unbound status underlying LTP. Indeed, an early

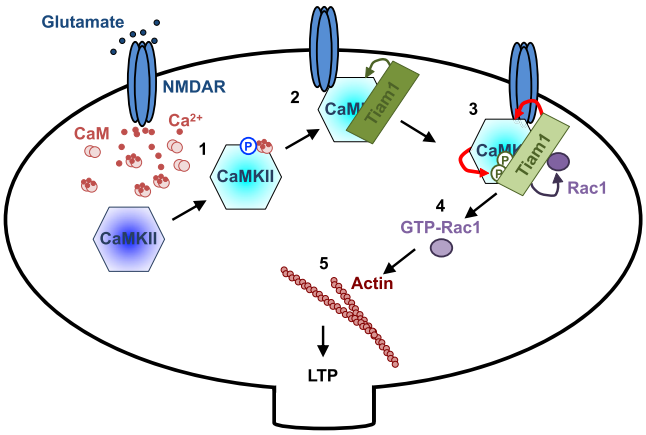

Figure 7. Schematic Model of RAKEC between Tiam1 and CaMKII for Persistence of sLTP

(1) Ca^{2+} influx through NMDAR increases Ca^{2+}/CaM binding to CaMKII, which activates the kinase and results in T286 autophosphorylation. Phosphorylated T286 disinhibits the kinase from autoinhibition. (2) Ca^{2+}/CaM-activated CaMKII binds to Tiam1 and NR2B subunit of NMDAR. Pseudo-autoinhibitory domain on Tiam1 dislodges the CaMKII autoinhibitory domain and prevents it from inhibiting the kinase. (3) In the protein complex with Tiam1, CaMKII phosphorylates and activates Tiam1 (RAKEC). This mechanism prolongs the kinase activity, which in turn maintains the phosphorylated status of Tiam1 and, therefore, its RacGEF activity. (4) Phosphorylated Tiam1 activates Rac1. (5) Rac1 promotes actin remodeling to maintain spine morphology.

Blue, inactive CaMKII; cyan, activated CaMKII; red arrows, reciprocal activation.

modeling study proposed that a positive feedback loop can sustain cellular signaling (Bhalla and Iyengar, 1999; Urakubo et al., 2014).

The proposed RAKEC mechanism maintains the activity of CaMKII/Tiam1 complex during LTP maintenance. This is contradictory to the previous work using a CaMKII FRET biosensor, Camui, which demonstrated that CaMKII activity increases only transiently during LTP induction and returns to basal level during maintenance (Lee et al., 2009). We believe this is because of the sensitivity the Camui probe. There are ~2,600 CaMKII dodecamers at single synapse, making CaMKII one of the most abundant postsynaptic proteins (Sheng and Hoogenraad, 2007; Feng et al., 2011). In contrast, most other signal-transduction molecules, such as Tiam1, are considerably less abundant (Sheng and Hoogenraad, 2007; Feng et al., 2011). Therefore, the proportion of CaMKII forming RAKEC with Tiam1 during LTP maintenance is expected to be small compared to the total amount of CaMKII. Additionally, biochemical studies detected basal CaMKII activity in unstimulated neuronal tissue (Barria et al., 1997; Yamagata et al., 2009). This background activity may mask the CaMKII that is activated by RAKEC mechanism in the Camui FRET measurement. Even though the FRET study shows CaMKII activity returns to the baseline level (Lee et al., 2009), the synaptic translocation of CaMKII (Shen and Meyer, 1999; Shen et al., 2000; Otmakhov et al., 2004; Bosch et al., 2014) would lead to a net increase in the number of active CaMKII molecules per synapse. This would account for the formation of the CaMKII RAKEC during LTP maintenance.

A report by Chang et al. (2017) showed that in T286A knockin mice, LTP was not induced using a standard LTP induction protocol. But with a stronger stimulation protocol, both structural and functional LTP could be induced, proposing that the phosphorylation of CaMKII on T286 is not required for LTP for maintenance. We found that the CaMKII phospho-block T286A can still form RAKEC between CaMKII and Tiam1 while phosphomimic T286D mutant enhances formation (Figures 4H and 5A), indicating that the T286 phosphorylation is facilitative to the formation of RAKEC but not an absolute requirement. Therefore, it is possible that a certain proportion of CaMKII remains active through RAKEC mechanism even in T286A context and maintains LTP in phospho-T286-independent manner.

In addition to temporal coding, we found that the Tiam1/CaMKII complex remained within the dendritic spine after sLTP inducing stimulation and did not diffuse to adjacent spines (Figures 3B and 3C). One explanation for this is that the interaction of CaMKII with other postsynaptic molecules such as NR2B maintains the Tiam1/CaMKII complex at the stimulated spine (Bayer et al., 2001; Barria and Malinow, 2005). CaMKII is an oligomeric enzyme that has been shown as dodecameric or tetradecameric (Chao et al., 2011; Bhattacharyya et al., 2016). Therefore, a single CaMKII holoenzyme can simultaneously interact with NR2B and Tiam1. Since CaMKII is turned on downstream of NMDAR activation, this would ensure assembly of binding partners only at the activated synapse. Given that the T-site interactions of CaMKII are required to enhance synaptic transmission by constitutively active CaMKII (Incontro et al., 2018), the importance of the T-site interaction would not only be for a kinase activity but also for localization or forming RAKEC. Therefore, CaMKII may function as a hub for both structural and cellular signaling.

At this point, it is not clear how much we can generalize the mechanism. The expression of Tiam1 is widespread and especially high in dentate granule cells, pyriform cortex, olfactory tubercle, and cerebellar granule cells (Allen Brain Atlas). Therefore, it is intriguing to test the involvement of Tiam1 in these regions.

An Atomic Model of the Interaction between CaMKII and Tiam1

At an atomic level, the interaction between CaMKII and Tiam1 was modeled using the X-ray crystal structure of a CaMKII kinase domain bound to CaMKIIN (Chao et al., 2010). Many of the residues in CaMKIIN important for the interaction are preserved in Tiam1 as well (Figure S3B). Mutation of those residues and their counterpart on CaMKII abolishes the binding (Figures 4C and 6C). However, it is curious that Tiam1 binding leads to activation while CaMKIIN binding causes inhibition. One possible explanation may be related to whether binding involves the S-site (substrate-binding site, located next to the T-site) or not. Most of the residues conserved between Tiam1 and CaMKIIN are located at the core consensus and N-terminal side, which interacts with the T-site (Figure S3B). There is less conservation at the C-terminal side of the binding region, which interacts with the S-site (Figure S3B). Because of this, Tiam1 binding may not interfere with the ability of substrates to bind the S-site, whereas CaMKIIN binding masks the S-site. Indeed, alanine substitutions on the C-terminal side of the binding region of Tiam1 did not affect binding to CaMKII (Figure 4C), whereas a similar manipulation of

CaMKIIN did diminish its inhibitory activity. Also, an S-site-binding peptide, Syntide 2, did not affect Tiam1 binding (Figure 4G). This difference in S-site interaction may explain the differential effects on kinase activity. Further studies to investigate this point will require more detailed atomic information of the interaction between Tiam1 and CaMKII.

Formation of RAKEC as a General Mechanism to Regulate the Spatial-Temporal Pattern of the Kinase Activity

There are several known CaMKII T-site-interacting proteins, including NR2B, ether à-go-go (eag) potassium channel (in *Drosophila*), GJD2/connexin 36, LRRC7/densin-180, and CaMKIIN, in addition to Tiam1 (Bayer et al., 2001; Walikonis et al., 2001; Sun et al., 2004; Vest et al., 2007; Alev et al., 2008). Indeed, the carboxyl tail of NR2B locks CaMKII in an active conformation independently of T286 autophosphorylation, which is necessary for LTP (Bayer et al., 2001; Barria and Malinow, 2005; Halt et al., 2012). Furthermore, a mass spectrometric study found that CaMKII interacts with multiple proteins, some of which might be mediated by the T-site as well. We propose that these interactors may also form RAKECs when CaMKII activity is temporally and spatially modulated, which in turn would maintain their phosphorylation state and, therefore, the cellular signaling they mediate. This study thus demonstrates that RAKECs can store biochemical information in small subcellular compartments and thus potentially serve as a mechanism to produce prolonged and compartmentalized signaling. Indeed, this revives an earlier view that CaMKII functions as a memory molecule (Lisman et al., 2002; Hell, 2014; Lisman, 2017).

Although Tiam1 specifically interacts with CaMKII but not with other members of the CaMK family (Figure 2D), autoinhibition is a common regulatory mechanism characteristic of many kinase families (Soderling, 1990; Huse and Kuriyan, 2002; Pufall and Graves, 2002). Therefore, it is possible that RAKECs represent a general mechanism for the regulation of specific cellular signaling pathways. Only effectors that can relieve autoinhibition can maintain the activated state of the kinase, thereby attaining spatiotemporal specificity of signaling and substrate specificity at the same time. In this way, the mechanism presented here provides a novel way to regulate specific cellular signaling cascades with precise spatiotemporal patterns.

STAR★METHODS

Detailed methods are provided in the online version of this paper and include the following:

- KEY RESOURCES TABLE
- CONTACT FOR REAGENT AND RESOURCE SHARING
- EXPERIMENTAL MODEL AND SUBJECT DETAILS
  - Animals
  - Cell culture
- METHOD DETAILS
  - Reagents
  - Plasmids
  - Lenti-virus production
  - 2-Photon laser-scanning microscopy and structural LTP induction
  - Chemical LTP
  - Immunoprecipitation from HEK293T cells
  - CaMKII activity induced by T-site interaction
  - GST-pull down assay
  - Pak-PBD pull-down assay
  - Rac1G15A pull-down assay
  - Phos-tag SDS-PAGE
  - Purification of CaMKII kinase domain for fluorescence polarization assay
  - Fluorescence polarization
- QUANTIFICATION AND STASTICAL ANALYSIS

SUPPLEMENTAL INFORMATION

Supplemental Information can be found online at https://doi.org/10.1016/j.neuron.2019.04.012.

ACKNOWLEDGMENTS

We would like to dedicate this work to the memory of John Lisman (1944–2017), who has always inspired us. We thank Drs. Karl Ulrich Bayer, Morgane Rosendale, and Lily Yu for comments on the manuscript. We also thank Drs. Mikoshiba and Eipper for providing anti-phospho-Homer3 antibody and Kalirin-7 construct, respectively. This work was supported by following agencies: RIKEN, RIKEN Presidents Fund (Y.H.); NIH grant R01DA17310 (Y.H.), DP1-NS096787 (R.Y.), R01-MH080047 (R.Y.); MEXT, Japan (20240032, 16H02455, 22110006, 18H04733 to Y.H.; 854508, 1031691, 374539, 817144 to T.S.); Human Frontier Science Programme (Y.H.); The Uehara Memorial Foundation (Y.H.); The Naito Foundation (Y.H.); The Takeda Science Foundation (Y.H., T.S.); Japan Foundation for Applied Enzymology (Y.H.); Novartis Foundation (Japan) for the Promotion of Science; Research Foundation for Opto-Science and Technology (Y.H.); Brain Science Foundation, Japan (Y.H.); Guangdong Key International Visiting Program, China (Y.H.); The Kyoto University Foundation (T.S.), The Shimadzu Science Foundation (T.S.), and The Pharmacological Research Foundation (T.S.).

AUTHOR CONTRIBUTION

T.S. and Y.H. conceived experiments and contributed funding. T.S. carried out biochemical and imaging experiments with assistance from A.S. and H. Matsuno. H. Murakoshi, N.G.H., and R.Y. contributed Rac1 sensor. E.A., R.O., and M.M.S. performed the fluorescent polarization assay. M.M.S. performed structural modeling. Y.H. and T.S. wrote the manuscript with help of others.

DECLARATION OF INTERESTS

Y.H. is partly supported by Takeda Pharmaceutical Co. Ltd., Fujitsu Laboratories, and Dwango.

Received: September 24, 2018
Revised: December 7, 2018
Accepted: April 3, 2019
Published: May 8, 2019

REFERENCES

Alev, C., Urschel, S., Sonntag, S., Zoidl, G., Fort, A.G., Höher, T., Matsubara, M., Willecke, K., Spray, D.C., and Dermietzel, R. (2008). The neuronal connexin36 interacts with and is phosphorylated by CaMKII in a way similar to CaMKII interaction with glutamate receptors. Proc. Natl. Acad. Sci. USA *105*, 20964–20969.

Barria, A., and Malinow, R. (2005). NMDA receptor subunit composition controls synaptic plasticity by regulating binding to CaMKII. Neuron *48*, 289–301.

Barria, A., Muller, D., Derkach, V., Griffith, L.C., and Soderling, T.R. (1997). Regulatory phosphorylation of AMPA-type glutamate receptors by CaM-KII during long-term potentiation. Science *276*, 2042–2045.

Bayer, K.U., De Koninck, P., Leonard, A.S., Hell, J.W., and Schulman, H. (2001). Interaction with the NMDA receptor locks CaMKII in an active conformation. Nature *411*, 801–805.

Bayer, K.U., LeBel, E., McDonald, G.L., O'Leary, H., Schulman, H., and De Koninck, P. (2006). Transition from reversible to persistent binding of CaMKII to postsynaptic sites and NR2B. J. Neurosci. *26*, 1164–1174.

Bhalla, U.S., and Iyengar, R. (1999). Emergent properties of networks of biological signaling pathways. Science *283*, 381–387.

Bhattacharyya, M., Stratton, M.M., Going, C.C., McSpadden, E.D., Huang, Y., Susa, A.C., Elleman, A., Cao, Y.M., Pappireddi, N., Burkhardt, P., et al. (2016). Molecular mechanism of activation-triggered subunit exchange in Ca^{2+}/calmodulin-dependent protein kinase II. eLife. Published online March 7, 2016. https://doi.org/10.7554/eLife.13405.

Bosch, M., and Hayashi, Y. (2012). Structural plasticity of dendritic spines. Curr. Opin. Neurobiol. *22*, 383–388.

Bosch, M., Castro, J., Saneyoshi, T., Matsuno, H., Sur, M., and Hayashi, Y. (2014). Structural and molecular remodeling of dendritic spine substructures during long-term potentiation. Neuron *82*, 444–459.

Chang, B.H., Mukherji, S., and Soderling, T.R. (1998). Characterization of a calmodulin kinase II inhibitor protein in brain. Proc Natl Acad Sci U S A *95* (18), 10890–10895.

Chang, J.Y., Parra-Bueno, P., Laviv, T., Szatmari, E.M., Lee, S.R., and Yasuda, R. (2017). CaMKII autophosphorylation is necessary for optimal integration of Ca2+ signals during LTP induction, but not maintenance. Neuron *94*, 800–808 e804.

Chao, L.H., Pellicena, P., Deindl, S., Barclay, L.A., Schulman, H., and Kuriyan, J. (2010). Intersubunit capture of regulatory segments is a component of cooperative CaMKII activation. Nat. Struct. Mol. Biol. *17*, 264–272.

Chao, L.H., Stratton, M.M., Lee, I.H., Rosenberg, O.S., Levitz, J., Mandell, D.J., Kortemme, T., Groves, J.T., Schulman, H., and Kuriyan, J. (2011). A mechanism for tunable autoinhibition in the structure of a human Ca^{2+}/calmodulin- dependent kinase II holoenzyme. Cell *146*, 732–745.

Coultrap, S.J., and Bayer, K.U. (2011). Improving a natural CaMKII inhibitor by random and rational design. PLoS ONE *6*, e25245.

Emsley, P., Lohkamp, B., Scott, W.G., and Cowtan, K. (2010). Features and development of Coot. Acta Crystallogr. D Biol. Crystallogr. *66*, 486–501.

Feng, B., Raghavachari, S., and Lisman, J. (2011). Quantitative estimates of the cytoplasmic, PSD, and NMDAR-bound pools of CaMKII in dendritic spines. Brain Res. *1419*, 46–52.

Fleming, I.N., Elliott, C.M., Buchanan, F.G., Downes, C.P., and Exton, J.H. (1999). Ca^{2+}/calmodulin-dependent protein kinase II regulates Tiam1 by reversible protein phosphorylation. J. Biol. Chem. *274*, 12753–12758.

Fortin, D.A., Davare, M.A., Srivastava, T., Brady, J.D., Nygaard, S., Derkach, V.A., and Soderling, T.R. (2010). Long-term potentiation-dependent spine enlargement requires synaptic Ca^{2+}-permeable AMPA receptors recruited by CaM-kinase I. J. Neurosci. *30*, 11565–11575.

García-Mata, R., Wennerberg, K., Arthur, W.T., Noren, N.K., Ellerbroek, S.M., and Burridge, K. (2006). Analysis of activated GAPs and GEFs in cell lysates. Methods Enzymol. *406*, 425–437.

Haditsch, U., Leone, D.P., Farinelli, M., Chrostek-Grashoff, A., Brakebusch, C., Mansuy, I.M., McConnell, S.K., and Palmer, T.D. (2009). A central role for the small GTPase Rac1 in hippocampal plasticity and spatial learning and memory. Mol. Cell. Neurosci. *41*, 409–419.

Halt, A.R., Dallapiazza, R.F., Zhou, Y., Stein, I.S., Qian, H., Juntti, S., Wojcik, S., Brose, N., Silva, A.J., and Hell, J.W. (2012). CaMKII binding to GluN2B is critical during memory consolidation. EMBO J. *31*, 1203–1216.

Harvey, C.D., Yasuda, R., Zhong, H., and Svoboda, K. (2008). The spread of Ras activity triggered by activation of a single dendritic spine. Science *321*, 136–140.

Hedrick, N.G., Harward, S.C., Hall, C.E., Murakoshi, H., McNamara, J.O., and Yasuda, R. (2016). Rho GTPase complementation underlies BDNF-dependent homo- and heterosynaptic plasticity. Nature *538*, 104–108.

Hell, J.W. (2014). CaMKII: claiming center stage in postsynaptic function and organization. Neuron *81*, 249–265.

Herring, B.E., and Nicoll, R.A. (2016). Kalirin and Trio proteins serve critical roles in excitatory synaptic transmission and LTP. Proc. Natl. Acad. Sci. USA *113*, 2264–2269.

Hosokawa, T., Mitsushima, D., Kaneko, R., and Hayashi, Y. (2015). Stoichiometry and phosphoisotypes of hippocampal AMPA-type glutamate receptor phosphorylation. Neuron *85*, 60–67.

Huse, M., and Kuriyan, J. (2002). The conformational plasticity of protein kinases. Cell *109*, 275–282.

Incontro, S., Díaz-Alonso, J., Iafrati, J., Vieira, M., Asensio, C.S., Sohal, V.S., Roche, K.W., Bender, K.J., and Nicoll, R.A. (2018). The CaMKII/NMDA receptor complex controls hippocampal synaptic transmission by kinase-dependent and independent mechanisms. Nat. Commun. *9*, 2069.

Ishida, A., and Fujisawa, H. (1995). Stabilization of calmodulin-dependent protein kinase II through the autoinhibitory domain. J. Biol. Chem. *270*, 2163–2170.

Kim, K., Lakhanpal, G., Lu, H.E., Khan, M., Suzuki, A., Hayashi, M.K., Narayanan, R., Luyben, T.T., Matsuda, T., Nagai, T., et al. (2015). A temporary gating of actin remodeling during synaptic plasticity consists of the interplay between the kinase and structural functions of CaMKII. Neuron *87*, 813–826.

Kwok, S., Lee, C., Sánchez, S.A., Hazlett, T.L., Gratton, E., and Hayashi, Y. (2008). Genetically encoded probe for fluorescence lifetime imaging of CaMKII activity. Biochem Biophys Res Commun. *69* (2), 519–525. Epub 2008 Feb 25. https://doi.org/10.1016/j.bbrc.2008.02.070.

Lee, S.J., Escobedo-Lozoya, Y., Szatmari, E.M., and Yasuda, R. (2009). Activation of CaMKII in single dendritic spines during long-term potentiation. Nature *458*, 299–304.

Lisman, J. (2017). Criteria for identifying the molecular basis of the engram (CaMKII, PKMzeta). Mol. Brain *10*, 55.

Lisman, J., Schulman, H., and Cline, H. (2002). The molecular basis of CaMKII function in synaptic and behavioural memory. Nat. Rev. Neurosci. *3*, 175–190.

Lois, C., Hong, E.J., Pease, S., Brown, E.J., and Baltimore, D. (2002). Germline transmission and tissue-specific expression of transgenes delivered by lentiviral vectors. Science *295*, 868–872.

Ma, X.M., Wang, Y., Ferraro, F., Mains, R.E., and Eipper, B.A. (2008). Kalirin-7 is an essential component of both shaft and spine excitatory synapses in hippocampal interneurons. J. Neurosci. *28*, 711–724.

Miller, P., Zhabotinsky, A.M., Lisman, J.E., and Wang, X.J. (2005). The stability of a stochastic CaMKII switch: dependence on the number of enzyme molecules and protein turnover. PLoS Biol. *3*, e107.

Mizutani, A., Kuroda, Y., Futatsugi, A., Furuichi, T., and Mikoshiba, K. (2008). Phosphorylation of Homer3 by calcium/calmodulin-dependent kinase II regulates a coupling state of its target molecules in Purkinje cells. J. Neurosci. *28*, 5369–5382.

Murakoshi, H., Shin, M.E., Parra-Bueno, P., Szatmari, E.M., Shibata, A.C., and Yasuda, R. (2017). Kinetics of endogenous CaMKII required for synaptic plasticity revealed by optogenetic kinase inhibitor. Neuron *94*, 37–47 e35.

Nicoll, R.A. (2017). A brief history of long-term potentiation. Neuron *93*, 281–290.

Noguchi, J., Hayama, T., Watanabe, S., Ucar, H., Yagishita, S., Takahashi, N., and Kasai, H. (2016). State-dependent diffusion of actin-depolymerizing factor/cofilin underlies the enlargement and shrinkage of dendritic spines. Sci. Rep. *6*, 32897.

Okamoto, K., Nagai, T., Miyawaki, A., and Hayashi, Y. (2004). Rapid and persistent modulation of actin dynamics regulates postsynaptic reorganization underlying bidirectional plasticity. Nat. Neurosci. *7*, 1104–1112.

Otmakhov, N., Tao-Cheng, J.H., Carpenter, S., Asrican, B., Dosemeci, A., Reese, T.S., and Lisman, J. (2004). Persistent accumulation of calcium/calmodulin-dependent protein kinase II in dendritic spines after induction of

NMDA receptor-dependent chemical long-term potentiation. J. Neurosci. *24*, 9324–9331.

Penzes, P., Cahill, M.E., Jones, K.A., and Srivastava, D.P. (2008). Convergent CaMK and RacGEF signals control dendritic structure and function. Trends Cell Biol. *18*, 405–413.

Pufall, M.A., and Graves, B.J. (2002). Autoinhibitory domains: modular effectors of cellular regulation. Annu. Rev. Cell Dev. Biol. *18*, 421–462.

Saneyoshi, T., and Hayashi, Y. (2012). The Ca^{2+} and Rho GTPase signaling pathways underlying activity-dependent actin remodeling at dendritic spines. Cytoskeleton (Hoboken) *69*, 545–554.

Saneyoshi, T., Wayman, G., Fortin, D., Davare, M., Hoshi, N., Nozaki, N., Natsume, T., and Soderling, T.R. (2008). Activity-dependent synaptogenesis: regulation by a CaM-kinase kinase/CaM-kinase I/betaPIX signaling complex. Neuron *57*, 94–107.

Shen, K., and Meyer, T. (1999). Dynamic control of CaMKII translocation and localization in hippocampal neurons by NMDA receptor stimulation. Science *284*, 162–166.

Shen, L., Liang, F., Walensky, L.D., and Huganir, R.L. (2000). Regulation of AMPA receptor GluR1 subunit surface expression by a 4. 1N-linked actin cytoskeletal association. J. Neurosci. *20*, 7932–7940.

Sheng, M., and Hoogenraad, C.C. (2007). The postsynaptic architecture of excitatory synapses: a more quantitative view. Annu. Rev. Biochem. *76*, 823–847.

Shutes, A., Onesto, C., Picard, V., Leblond, B., Schweighoffer, F., and Der, C.J. (2007). Specificity and mechanism of action of EHT 1864, a novel small molecule inhibitor of Rac family small GTPases. J. Biol. Chem. *282*, 35666–35678.

Soderling, T.R. (1990). Protein kinases. Regulation by autoinhibitory domains. J. Biol. Chem. *265*, 1823–1826.

Sun, X.X., Hodge, J.J., Zhou, Y., Nguyen, M., and Griffith, L.C. (2004). The eag potassium channel binds and locally activates calcium/calmodulin-dependent protein kinase II. J. Biol. Chem. *279*, 10206–10214.

Takao, K., Okamoto, K., Nakagawa, T., Neve, R.L., Nagai, T., Miyawaki, A., Hashikawa, T., Kobayashi, S., and Hayashi, Y. (2005). Visualization of synaptic Ca^{2+} /calmodulin-dependent protein kinase II activity in living neurons. J. Neurosci. *25*, 3107–3112.

Tashiro, A., Minden, A., and Yuste, R. (2000). Regulation of dendritic spine morphology by the rho family of small GTPases: antagonistic roles of Rac and Rho. Cereb. Cortex *10*, 927–938.

Tolias, K.F., Bikoff, J.B., Burette, A., Paradis, S., Harrar, D., Tavazoie, S., Weinberg, R.J., and Greenberg, M.E. (2005). The Rac1-GEF Tiam1 couples the NMDA receptor to the activity-dependent development of dendritic arbors and spines. Neuron *45*, 525–538.

Um, K., Niu, S., Duman, J.G., Cheng, J.X., Tu, Y.K., Schwechter, B., Liu, F., Hiles, L., Narayanan, A.S., Ash, R.T., et al. (2014). Dynamic control of excitatory synapse development by a Rac1 GEF/GAP regulatory complex. Dev. Cell *29*, 701–715.

Urakubo, H., Sato, M., Ishii, S., and Kuroda, S. (2014). In vitro reconstitution of a CaMKII memory switch by an NMDA receptor-derived peptide. Biophys. J. *106*, 1414–1420.

Vest, R.S., Davies, K.D., O'Leary, H., Port, J.D., and Bayer, K.U. (2007). Dual mechanism of a natural CaMKII inhibitor. Mol. Biol. Cell *18*, 5024–5033.

Walikonis, R.S., Oguni, A., Khorosheva, E.M., Jeng, C.J., Asuncion, F.J., and Kennedy, M.B. (2001). Densin-180 forms a ternary complex with the (α)-subunit of Ca^{2+}/calmodulin-dependent protein kinase II and (α)-actinin. J. Neurosci. *21*, 423–433.

Wiens, K.M., Lin, H., and Liao, D. (2005). Rac1 induces the clustering of AMPA receptors during spinogenesis. J. Neurosci. *25*, 10627–10636.

Xie, Z., Srivastava, D.P., Photowala, H., Kai, L., Cahill, M.E., Woolfrey, K.M., Shum, C.Y., Surmeier, D.J., and Penzes, P. (2007). Kalirin-7 controls activity-dependent structural and functional plasticity of dendritic spines. Neuron *56*, 640–656.

Yamagata, Y., Kobayashi, S., Umeda, T., Inoue, A., Sakagami, H., Fukaya, M., Watanabe, M., Hatanaka, N., Totsuka, M., Yagi, T., et al. (2009). Kinase-dead knock-in mouse reveals an essential role of kinase activity of Ca2+/calmodulin-dependent protein kinase IIalpha in dendritic spine enlargement, long-term potentiation, and learning. J. Neurosci. *29*, 7607–7618.

Zhabotinsky, A.M. (2000). Bistability in the $Ca^{(2+)}$/calmodulin-dependent protein kinase-phosphatase system. Biophys. J. *79*, 2211–2221.

STAR★METHODS

KEY RESOURCES TABLE

REAGENT or RESOURCE	SOURCE	IDENTIFIER
Antibodies		
Mouse monoclonal anti-Flag-M2 antibody	Sigma-Aldrich	Cat#. F1804; RRID: AB_439685
Flag-M2 agarose	Sigma-Aldrich	Cat#. A2220; RRID: AB_439685
Rabbit polyclonal anti-Tiam1 C16	Santa-Cruz Biotechnology	Cat#. Sc-872; RRID: AB_2240410
Rabbit polyclonal anti-Tiam1 N15	Santa-Cruz Biotechnology	Cat#. Sc-871; RRID: AB_2201571
Sheep polyclonal anti-Tiam1	R&D systems	Cat#. AF-5038; RRID: AB_2303175
Mouse monoclonal anti-CaMKII (G-1)	Santa-Cruz Biotechnology	Cat#. Sc-5306; RRID: AB_626788
Rabbit anti-phosphor-CaMKII T286	Santa-Cruz Biotechnology	Cat#. Sc-12886
Mouse monoclonal anti-Myc-9E10 antibody	Santa-Cruz Biotechnology	Cat#. Sc-40; RRID: AB_627268
Mouse monoclonal anti-GST antibody (GS019)	Nacalai Tesque	Cat#. 04435-26
Mouse monoclonal anti-Rac1 antibody (clone 102)	BD Bioscience	Cat#. 610651; RRID: AB_397978
Mouse monoclonal anti-MAP2 antibody (HM2)	Novus Biologicals	Cat#. #NB120-11267; RRID: AB_2138179
Goat polyclonal anti-Kalirin-7 antibody	Novus Biologicals	Cat#. #NB100-41371; RRID: AB_2128148
Rabbit polyclonal anti-βPIX antibody	Cell Signaling Technologies	Cat#. #4515S; RRID: AB_2274365
Rabbit polyclonal anti-Phosphorylate Homer3 S120	Mizutani et al., 2008	N/A
Rabbit polyclonal anti- Phospho-(Ser/Thr) Akt Substrate Antibody	Cell Signaling Technologies	Cat#. #9611S; RRID: AB_330302
Alexa647-goat anti-mouse IgG	Invitrogen	Cat#. A21236; RRID: AB_2535805
Alexa594-goat anti-rabbit IgG	Invitrogen	Cat#. A11037; RRID: AB_2534095
Alexa546-donkey anti-goat IgG	Invitrogen	Cat#. A11056; RRID: AB_2534103
Anti-mouse IgG HRP-linked whole Ab Sheep	GE Healthcare	Cat#. NA931-1ML; RRID: AB_772210
Anti-rabbit IgG HRP-linked whole Ab donkey	GE Healthcare	Cat#. NA934-1ML; RRID: AB_772206
Anti-sheep IgG HRP-linked	Invitrogen	Cat#. A16041; RRID: AB_2534715
Bacterial and Virus Strains		
Lenti-FUGHW-shTiam1-Tiam1-Flag WT	This paper	N/A
Lenti-FUGHW-shTiam1-Tiam1-Flag AAA	This paper	N/A
Chemicals, Peptides, and Recombinant Proteins		
Tetrodotoxin	Latoxan laboratory	Cat#. L8503
Picrotoxin	Nacalai tesque	Cat#. 28004-71
MNI-caged glutamate	Tocris	Cat#. 1490
KN-93	Tocris	Cat#. 1278
EHT1864	Tocris	Cat#. 3872
AP-5	Tocris	Cat#. 0106
Phostag acrylamide	FUJIFILM Wako Pure Chemical Corporation	Cat#. AAL-107
PEI max	Polyscience, Inc	Cat#. 24765-1
Tiam1 CBD: RTLDSHASRMTQLKKQAALSG	This paper	N/A
Tiam1 CBD scrambled: HLRMRLGSAKSQSTKLATADQ	This paper	N/A
Experimental Models: Cell Lines		
Human: HEK293T cell	ATCC	CRL3216
Experimental Models: Organisms/Strains		
Rat; SD.	SLC	N/A

(*Continued on next page*)

Continued

REAGENT or RESOURCE	SOURCE	IDENTIFIER
Recombinant DNA		
pmGFP-Rac1	Hedrick et al., 2016	N/A
pmCherry-PBD-mCherry	Hedrick et al., 2016	N/A
pSuper-shTiam1	Tolias et al., 2005	N/A
pSuper-shKalirin-7	Ma et al., 2008	N/A
pmU6pro-sh-betaPIX	Saneyoshi et al., 2008	N/A
pCAGGS-mGFP	This paper	N/A
pCAGGS-Tiam1-Flag	This paper	N/A
pCAGGS-Kalirin-7-Flag	This paper	Addgene plasmid#25454
pCAGGS-betaPIX-Flag	Saneyoshi et al., 2008	N/A
pCAGGS-Myc-CaMKI-alpha	Saneyoshi et al., 2008	N/A
pCAGGS-Myc-CaMKII-alpha	Saneyoshi et al., 2008	N/A
pCAGGS-Myc-CaMKIV	Saneyoshi et al., 2008	N/A
pCAGGS-Myc-CaMKK-alpha	Saneyoshi et al., 2008	N/A
pCAGGS-mCherry-CaMKII-alpha-mCherry	This paper	N/A
pCAGGS-Tiam1-EGFP	This paper	N/A
pCS2-Flag-Tiam1 1540-1591	This paper	N/A
pCAGGS-CaMKII-alpha-myc wild-type	This paper	N/A
pCAGGS-CaMKII-alpha-myc F98K	This paper	N/A
pCAGGS-CaMKII-alpha-myc E139R	This paper	N/A
pCAGGS-CaMKII-alpha-myc I205K	This paper	N/A
pCAGGS-CaMKII-alpha-myc W237K	This paper	N/A
pCAGGS-CaMKII-alpha-myc K42R	This paper	N/A
pCAGGS-CaMKII-alpha-myc T286A	This paper	N/A
pCAGGS-CaMKII-alpha-myc T286D	This paper	N/A
pCAGGS-CaMKII-alpha-myc K42R,T286D	This paper	N/A
pCAGGS-CaMKII-alpha-myc T305DT306D	This paper	N/A
pCAGGS-CaMKII-alpha-myc 1-290	This paper	N/A
pFHUGW-shLuc-LacZ-Flag	This paper	N/A
pFHUGW-shTiam1-LacZ-Flag	This paper	N/A
pFHUGW-shTiam1-Tiam1-Myc WT	This paper	N/A
pFHUGW-shTiam1-Tiam1-Myc AAA	This paper	N/A
p-mRFP1CaMKII-alpha-mGFP (camui)	Kwok et al., 2008	N/A
pJPA-CaMKIIN	Chang et al., 1998	N/A
pmCherry-PA-AIP2	Murakoshi et al., 2017	N/A
GST	pGEX4T1, GE healthcare	Cat#. 28954549
GST-Tiam1 421-1591	This paper	N/A
GST-Tiam1 421-852	This paper	N/A
GST-Tiam1 840-1025	This paper	N/A
GST-Tiam1 1025-1591	This paper	N/A
GST-Tiam1 1540-1591	This paper	N/A
Flag peptide	Sigma-Aldrich	Cat#. F3290
Syntide2	Calbiochem	Cat#. 05-23-4910
AC3	Anaspec Inc.	Cat#. 64927
AIP	Anaspec Inc.	Cat#. 64926
CaMKIINtide	Calbiochem	Cat#. 208920
CBD	This paper	N/A
CBD scrambled	This paper	N/A
GST-Pak1RBD	Saneyoshi et al., 2008	N/A

(*Continued on next page*)

Continued

REAGENT or RESOURCE	SOURCE	IDENTIFIER
GST-Rac1 G15A	This paper	N/A
Lambda protein phosphatese	NEB	P0753S
GST-AC2	This paper	N/A
GST-Homer3	Mizutani et al., 2008	N/A
Software and Algorithms		
Igor Pro	Bosch et al., 2014	https://www.wavemetrics.com/
Statcel2	OMS publishing Inc.	N/A
KaleidaGraph	This paper	http://www.synergy.com/wordpress_650164087/kaleidagraph/
ImageJ	Bosch et al., 2014	https://imagej.nih.gov/nih-image/

CONTACT FOR REAGENT AND RESOURCE SHARING

Further information and requests for resources and reagents should be directed to and will be fulfilled by the Lead Contact, Takeo Saneyoshi (saneyoshi.takeo.3v@kyoto-u.ac.jp).

EXPERIMENTAL MODEL AND SUBJECT DETAILS

All experimental protocols were approved by the RIKEN and Kyoto University Committee for Animal Care guidelines.

Animals

Rats from Sprague-Dawley strain (purchased Japan SLC, both males and females) were used for hippocampal slice culture and dissociated neuronal cultures.

Cell culture

HEK293T cells were cultured at 37°C in Dulbecco's modified Eagle's medium supplemented with 10% fetal bovine serum. Transfections were performed using the PEI max (Polysciences, PA, USA). Hippocampal slices and dissociated neuronal cultured were prepared as described (Bosch et al., 2014). P6-8 and P0-1 Sprague-Dawley rats (both males and females) were used for slice culture and dissociated culture, respectively. Slices were transfected by a biolistic method (Gene-Gun, Bio-Rad, CA, USA). Dissociated neurons were infected using lentivirus vector (Bosch et al., 2014).

METHOD DETAILS

Reagents

KN-93, bicuculline, strychnine, D-(-)-2-Amino-5-phosphonopentanoic acid (AP5), and MNI-caged-L-glutamate were from Tocris Bioscience (Bristol, UK); TTX from Latoxan (Valence, France) or Wako (Osaka, Japan); Glutathione agarose (GST-Accept) from Nacalai Tesque (Kyoto, Japan); Phos-tag acrylamide from Wako; Syntide 2, AC3, AIP, and CaMKIINtide were from Merck-Millipore (Darmstadt, Germany). CaMKII-binding-peptide of Tiam1, RTLDSHASRMTQLKKQAALSG, and its randomized sequence, HLRMRLGSAKSQSTKLATADQ, fluorescein-RTLDSHASRMTQLKKQAA-amide were synthesized in the Research Resource Center of RIKEN Brain Science Institute.

CaMKII (clone G1), phosphorylated T-286 CaMKII, Tiam1 (clones N15, C16), and Myc (clone 9E10) were purchased from Santa Cruz (TX, USA). CaMKII (clone 45) and Rac1 (clone 102) from BD Bioscience (NJ, USA). Anti-Tiam1 from sheep from R&D systems (MN, USA). Flag-M2 monoclonal antibody and Flag-M2-agarose from Sigma (MO, USA). Anti-MAP2 (HM2) and anti-Kalirin-7 antibodies from Novus Biologicals (CO, USA). GST antibody from Nacalai. Rabbit anti-phospho-S120 Homer3 antibody (Mizutani et al., 2008) was a kind gift from Dr. Katsuhiko Mikoshiba.

Plasmids

Tiam1 cDNA was isolated from mouse cDNA library. Rac1 biosensor was reported previously (Hedrick et al., 2016). For Tiam1 molecular replacement experiment (Figures 6E–6G), shRNA for Tiam1 was subcloned into FHUGW and GFP was replaced with mCherry-Pak2 Rac1/Cdc42 binding domain (RBD) (with R71C, S78A mutations)-mCherry. The shRNA sequences are follows: For Tiam1, GAGGGAGAAGGAAGTGGTC (Tolias et al., 2005), luciferase, GTACGCGGAATACTTCGA (Bosch et al., 2014), Kalirin-7, TACTTGAGTTGCAGACTTT (Ma et al., 2008), βPIX, GGTAGTACGAGCCAAGTTT (Saneyoshi et al., 2008). shRNAs were subcloned in pSuper (Oligoengine), pmU6pro, or FHUGW (Lois et al., 2002). For Tiam1 lentivirus production, shRNA for Tiam1 was subcloned

into FHUGW, and GFP was replaced with shRNA-resistant Tiam1 wild-type or AAA mutant. Flag-tagged Kalirin-7 was generated from pEAK10-His-Myc-Kal7 (Addgene plasmid # 25454). Flag-tagged βPIX, CaMKIα, CaMKIIα, CaMKIV, and CaMKKα were described previously (Saneyoshi et al., 2008). CaMKII mutants, Tiam1 fragments and mutants were made by standard method.

Lenti-virus production

HEK293T cells were transfected with FHUGW plasmids along with pCAG_HIV_gp and pCMV_VSVG_RSV-Rev vectors using PEI method (Kim et al., 2015). Virus-containing culture supernatants were concentrated by ultracentrifugation. Virus solutions were aliquoted and kept at −80°C until use.

2-Photon laser-scanning microscopy and structural LTP induction

Imaging was carried out with a two-photon microscope (FV1000-MPE, Olympus, Tokyo, Japan) with Ti-sapphire lasers (Spectra-Physics, CA, USA). Fluorescent lifetime was measured as previously described (Bosch et al., 2014) using time-correlated photon-counting technology (SPC-830, Becker and Hickl, Berlin, Germany; H7422P-40, Hamamatsu Photonics, Hamamatsu, Japan) at 910 nm excitation. Detection was synchronized with excitation light pulses using an external detector. Emission light was filtered with a 680 nm short-pass and 510/70 nm band-pass filters. Bleed-through of the acceptor fluorescence into the emission channel was negligible. The lifetime images were analyzed using a custom written macro in Igor-Pro (Wavemetrics, OR, USA). Averaged fluorescence lifetime in the spine head was calculated and presented as the difference from baseline (Bosch et al., 2014). For experiments visualizing Rac1 activity, neurons were cultured in extra $MgCl_2$ (final concentration 10.8 mM) on the day before imaging as previously described (Harvey et al., 2008).

Hippocampal organotypic slice cultures 5-12 days in culture (DIV) were transfected with plasmids at the following ratio; for Rac1 activity imaging, mEGFP-Rac1:mCherry-Pak2-RBD-mCherry at 1:2 ratio and for detection of Tiam1-CaMKII interaction, Tiam1-mEGFP:mCherry-CaMKIIα-mCherry at 1:4 ratio. All imaging experiments were carried out at 30°C in Mg^{2+}-free artificial cerebral spine fluid (ACFS) containing 4 mM $CaCl_2$, 1 μM tetrodotoxin, 50 μM picrotoxin, and 2.5 mM MNI-caged-L-glutamate aerated with 95% O_2 and 5% CO_2. Imaging was performed at 8-16 DIV in primary or secondary dendrites from the distal part of the main apical dendrite of CA1 pyramidal neurons. We induced structural LTP on spines with a clear head and neck by uncaging MNI-glutamate with 2 to 6 ms laser pulses (720 nm at 5 mW under objective lens) repeated at 0.5 or 1 Hz for 30 pulses. The sLTP stimulation with 0.5 Hz for 30 pulses were used for Camui and Tiam1/CaMKII imaging in Figure 3E, and Rac1 activity imaging. For other experiments, 1 Hz for 30 pulses was used to induce sLTP.

For photoactivation of paAIP2 experiment, we monitored structure with GFP fluorescence or Tiam1-GFP as a proxy. Images were taken at 1010 nm to avoid photoactivation of paAIP2. Photoactivation was applied using 473 nm laser (100 mW/cm^2, Shanghai Laser, Shanghai, China) with 200 ms pulses at 1 Hz for 1 min.

Chemical LTP

Chemical LTP was performed as describe (Fortin et al., 2010; Bosch et al., 2014). Dissociated hippocampal neurons at 14 to 21 DIV were preincubated with HEPES-based ACSF (130 mM NaCl, 2.5 mM KCl, 0 mM Mg^{2+}, 2 mM $CaCl_2$, 25 mM HEPES [pH 7.3], 30 mM glucose, 310-320 mOsm/L), containing 1 μM tetrodotoxin for 30 min. Neurons were stimulated with ASCF supplemented with 200 μM glycine, 20 μM bicuculline, 3 μM strychnine for 10 min, then returned to ACSF without glycine.

Immunoprecipitation from HEK293T cells

HEK293T cell lysates were prepared in lysis buffer (50 mM Tris-HCl [pH 8.0], 150 mM NaCl, 1% Triton X-100, 10% glycerol, 1 mM Na_3VO_4, 10 mM NaF, 1 mM β-glycerophosphate, 1 x phosphatase inhibitor cocktail [Nacalai], 1 x complete tablet [Roche, Basel, Switzerland]) and centrifugation at 10,000 x g for 10 min at 4°C. The supernatant was subjected to immunoprecipitation using 10 μL of the anti-Flag antibody-beads (Sigma) for 2-4 hours at 4°C. Beads were washed with 1 mL of lysis buffer for three times. Bound proteins were eluted with SDS-PAGE sample buffer or Flag-peptide and subjected to western blotting.

CaMKII activity induced by T-site interaction

Flag-tagged human CaMKIIα wild-type and T286A were purified from HEK293T cell using FlagM2-agarose. After elution with Flag peptide, concentration of CaMKII was quantified by western blotting using purified CaMKIIβ protein as a standard (Kim et al., 2015). Kinase assay was performed according to Bayer et al. (2001). GST or GST-Tiam1-1540-1591 were preincubated for 12 min at 30°C with CaMKII (100 nM CaMKII, 10 μM GST or GST-Tiam1-1540-1591 protein, 4.5 μM calmodulin, 10 mM PIPES pH 7.0, 0.1 mg/mL BSA, 0.25 mM $CaCl_2$). EGTA was added to a final concentration of 2.5 mM, and samples were used for kinase reaction. Kinase reaction was performed for 30 min at 30°C using 20 nM CaMKII from above reaction and 5 μg of GST-Homer3 as substrate (Mizutani et al., 2008), in a buffer containing 50 mM HEPES (pH 7.5), 10 mM $MgCl_2$, 2.5 mM DTT, 0.005% Tween 20, 0.1 mg/mL BSA, 50 μM ATP, and either 1 mM $CaCl_2$ and 1.5 μM calmodulin or 5 mM EGTA. The reaction was stopped by adding SDS-PAGE sample buffer.

GST-pull down assay

Ten μg of GST or GST-fusion proteins were immobilized on 25 μl of glutathione-agarose. HEK293T cell lysates were added to the beads, and incubated for 2 hours at 4°C. After washing, bound proteins were extracted with SDS-PAGE sample buffer and detected by western blotting.

Pak-PBD pull-down assay

GST-Pak1-p21 binding domain (PBD) was prepared from bacteria as previously described (Saneyoshi et al., 2008). For Pak-PBD pull-down assay, HEK293T cells were detached by trypsin/EDTA (Nacalai) before cell lysis. Soluble cell lysate was prepared in 1 mL of BOS lysis buffer (1% NP40, 50 mM Tris-HCl [pH 7.5], 200 mM NaCl, 10 mM $MgCl_2$, 10% glycerol, 1 x Complete EDTA-free tablet [Roche], 1 x phosphatase inhibitor cocktail [Nacalai]), supplemented with 40 μg/mL of GST-Pak1-PBD per 10-cm diameter culture dish (Corning, NY, USA). Soluble cell extracts were incubated with 25 μl of glutathione-agarose for 30 min at 4°C, and washed three times with BOS lysis buffer. Bound activated endogenous Rac1 was detected by western blotting using Rac1 antibody.

Rac1G15A pull-down assay

GST-Rac1G15A protein was prepared from bacterial strain BL21(DE3)pLysS as previously described (Saneyoshi et al., 2008). After chemical LTP was induced, dissociated hippocampal lysates were prepared in deoxycholate lysis buffer (50 mM Tris-HCl [pH 8.5], 150 mM NaCl, 1% deoxycholate, 5 mM $MgCl_2$, 10% Glycerol, 1 mM Na_3VO_4, 10 mM NaF, 1 mM β-glycerophosphate, 1 x phosphatase inhibitor cocktail [Nacalai], 1 x Complete tablet [Roche]), and centrifuged at 20,000 x g for 10 min at 4°C. Soluble fractions were incubated with 10 μg of GST-Rac1G15A immobilized on glutathione-agarose for 2-4 hours at 4°C and washed three times with deoxycholate lysis buffer. Bound activated Tiam1 was detected by western blotting using Tiam1 antibody.

Phos-tag SDS-PAGE

Five % acrylamide gel, 15 μM of $MnCl_2$ and 7.5 μM of Phos-tag acrylamide (AAL-107, Wako) (Figures 5D and 5E), or 5% acrylamide gel with 10 μM of $MnCl_2$ and 7.5 μM Phos-tag acrylamide (Figure 5F) were used (Hosokawa et al., 2015). The samples were separated by electrophoresis using the gels above. The gels were washed with 20 mM EDTA to remove Mn^{2+} before western blotting.

Purification of CaMKII kinase domain for fluorescence polarization assay

Human CaMKIIα kinase domain was expressed using *E. coli,* and prepared as described previously (Chao et al., 2010). Briefly, the cDNA fragment (amino acids 6-274 with D135N mutation) was subcloned in a pSMT-3 vector containing an N-terminal sumo expression tag (LifeSensors, Pennsylvania, PA) and protein expression was done in BL21(DE3)pLysS cells. Protein expression was induced by addition of 1 mM isopropyl β-D-1-thiogalactopyranoside and grown overnight at 18°C. All subsequent purification steps were carried out at 4°C. Cell pellets were resuspended in Buffer A (25 mM Tris, pH 8.5, 150 mM potassium chloride (KCl), 1 mM DTT, 50 mM imidazole, and 10% glycerol) and lysed using a cell disrupter. Cleared lysate was loaded on a 5 mL Ni-NTA column, eluted with 0.5 M imidazole, desalted using a HiPrep 26/10 desalting column into Buffer A with 0 mM imidazole and 2 mM tris(2-carboxyethyl)phosphine) (TCEP), and cleaved with Ulp1 protease overnight. The cleaved samples were loaded onto the Ni-NTA column and the flow through was loaded onto a Q-FF 5 mL column, and then eluted with a KCl gradient. Eluted proteins were concentrated and then further purified using a Superdex 200 gel-filtration column equilibrated in 25 mM Tris, pH 8.0, 150 mM KCl, 2 mM TCEP and 10% glycerol. Fractions with purified protein (> 95% pure) were frozen at −80°C. All columns were purchased from GE Healthcare (Piscataway, NJ).

Fluorescence polarization

The fluorescence polarization experiments were carried out by adding 10 μL of 120 nM fluorescein-labeled Tiam1 peptides (fluorescein-RTLDSHASRMTQLKKQAA-amide dissolved in 25 mM Tris pH 7.5, 150 mM KCl, 0.02% Tween, 0.02% Triton) to 10 μL D135N CaMKII kinase domain at varying concentrations (25 mM Tris pH 7.5, 150 mM KCl, 10% glycerol, 1 mM TCEP). A Synergy H1 hybrid plate reader (Biotek) was then used to measure the fluorescence polarization with a filter of 485/20 nm excitation and 528/20 nm emission. Error bars were calculated from the standard error of mean between replicates. Data were fit using a single-site binding equation (Bhattacharyya et al., 2016):

$$y = K1 + \frac{(K2 - K1) \times \left(([CaMKII] + K3 + [peptide]) - \sqrt{([CaMKII] + K3 + [peptide])^2 - 4 \times K3 \times [peptide]} \right)}{2 \times [peptide]}$$

where,

[*CaMKII*]: concentration of monomeric kinase domain of CaMKII, varied from 0 to 7.5×10^{-5} M.

and

[*peptide*]: concentration of Tiam1 peptide, fixed at 6×10^{-8} M.

Modeling of Tiam1 peptide and CaMKII kinase domain

We used Coot (Emsley et al., 2010) to create the Tiam1 peptide using CaMKIIN as a model and performed a global energy minimization of the peptide itself. We then modeled the Tiam1 peptide onto the CaMKII kinase domain using the crystal structure of CaMKII bound to CaMKIIN as a starting point (Chao et al., 2010), The modeled peptide was docked onto the CaMKII kinase domain using PyMol, and side chain orientations were adjusted to mimic the CaMKIIN interaction mode.

QUANTIFICATION AND STASTICAL ANALYSIS

Quantification results were expressed as the mean ± SEM. The statistical significance of the results was assessed by analysis of variance (ANOVA) with post hoc comparisons using the Tukey's HSD test or Dunnett's test, Wilcoxon signed-rank test, or two-tailed Student's t test using Statcel2 for Excel (Microsoft) or KaleidaGraph (Synergy Software). For all tests of statistical significance, $p < 0.05$ was considered significant.

For spine imaging quantification, numbers of observation represent the spine number which was imaged from single neurons. In western blot analysis, number represents numbers of independent experiments.

Neuron, Volume *102*

Supplemental Information

Reciprocal Activation within a Kinase-Effector Complex Underlying Persistence of Structural LTP

Takeo Saneyoshi, Hitomi Matsuno, Akio Suzuki, Hideji Murakoshi, Nathan G. Hedrick, Emily Agnello, Rory O'Connell, Margaret M. Stratton, Ryohei Yasuda, and Yasunori Hayashi

Fig. S1. Saneyoshi et al.

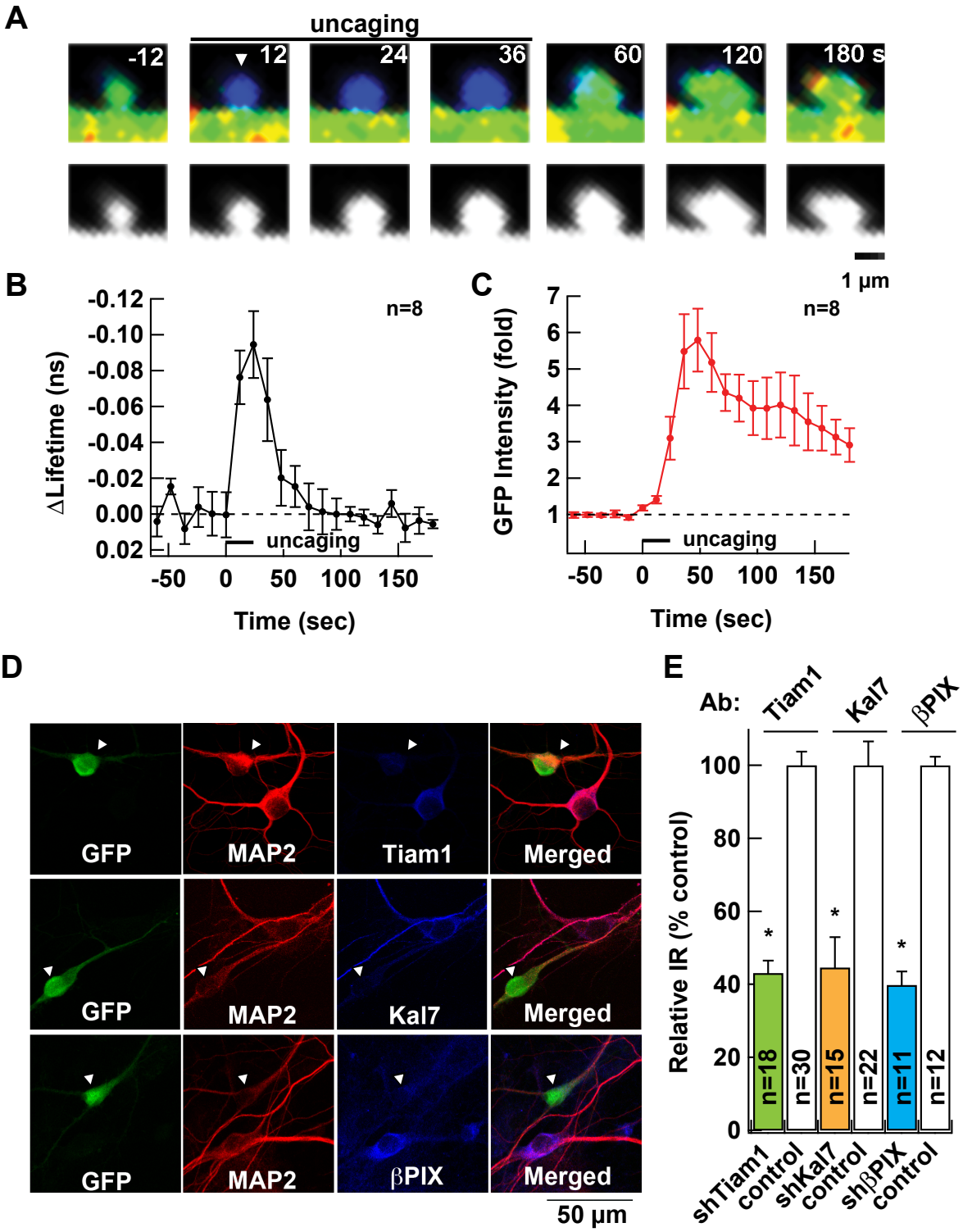

Figure S1, related to Figures 1 and 2. Activation of CaMKII during sLTP is transient in hippocampal organotypic slice culture and efficacy of shRNA against the RacGEF.

A. Activation of CaMKII as visualized by FRET-FLIM-based CaMKII activity sensor, Camui, during sLTP. CaMKII activity and distribution of Camui sensor, as a proxy of structure, are shown. Cooler colour hues in FLIM images indicates higher CaMKII activity.

B, C. Summary of CaMKII activity (B) and volume of the spine (C).

D, E. Test of efficiency of shRNA against the RacGEFs. Hippocampal dissociated neurons were transfected with GFP and shRNA construct against Tiam1, Kalirin-7 (Kal7), or βPIX. Four days after transfection, neurons were fixed and stained with antibodies against RacGEFs (Tiam1, Kal7, or βPIX), MAP2, and Hoechst 33342 (D). Arrow heads indicate GFP positive cells. Quantification of RacGEF protein in shRNA expressing neuron (E). Immunoreactivities (IR) were compared with a GFP positive neuron and its neighbor cell: both cells were MAP2 positive. Relative IR were normalized to MAP2 positive/GFP negative cells as 100% (control). *, $p < 0.05$, compared to control; *t*-test.

Data are represented as mean ± SEM (B, C, E).

Fig. S2. Saneyoshi et al.

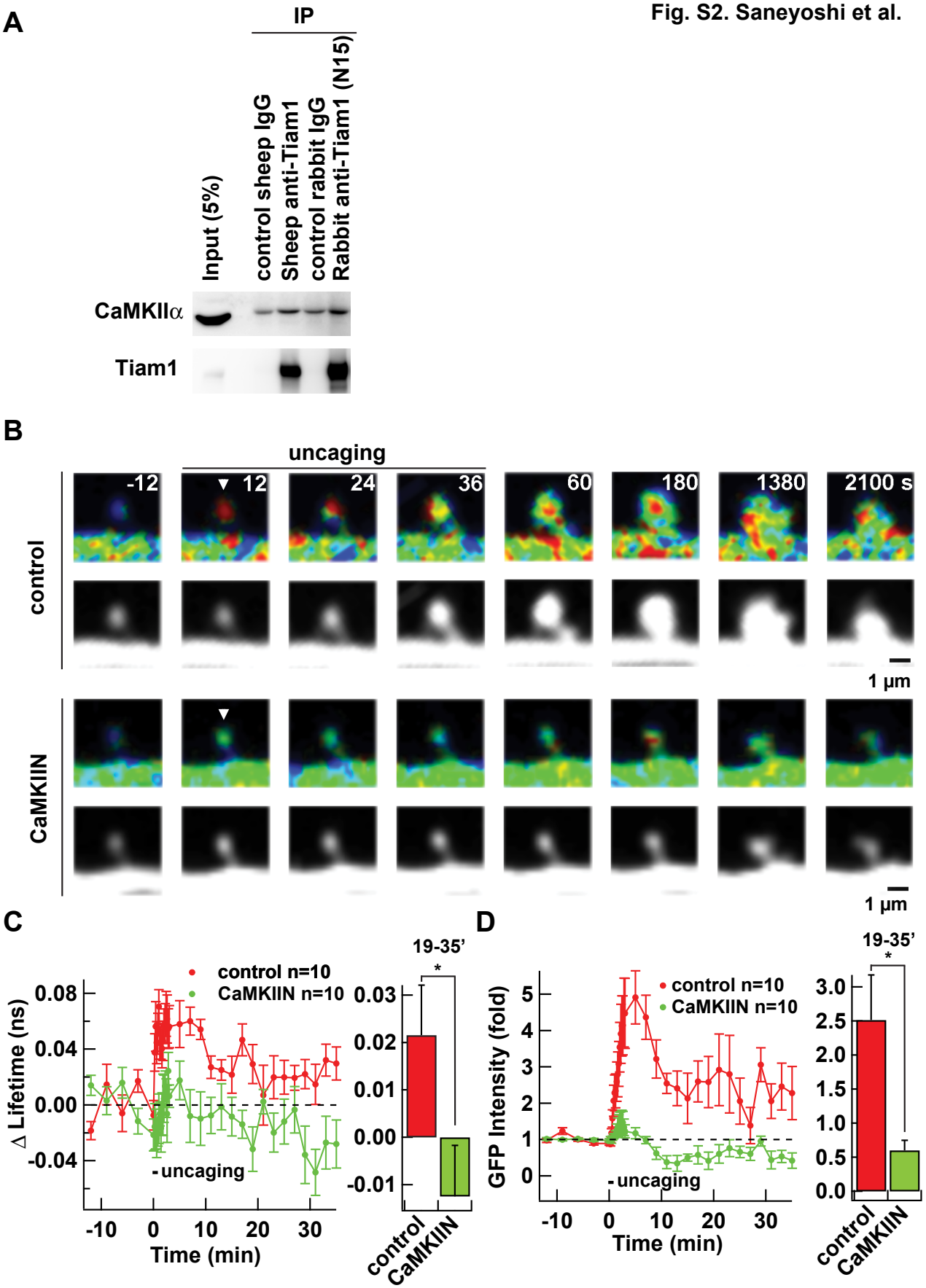

18

Figure S2, related to Figure 3. Interaction between Tiam1 and CaMKII and effect of CaMKIIN overexpression

A. Co-immunoprecipitation between Tiam1 and CaMKII from brain tissue. Whole brain lysate was immunoprecipitated with control IgG (Sheep or Rabbit) or anti-Tiam1 antibodies and protein-G sepharose. After extensive wash, immuprecipitated proteins (IP) were eluted with SDS-PAGE sample buffer, and then subjected to western blotting using Tiam1 and CaMKII antibodies.

B. Representative images of the interaction between Tiam1 and CaMKII with or without CaMKIIN overexpression. Other conventions are similar to Fig. 1.

C, D. Summary of FRET change (C) and volume (D) from multiple spines. *, $p < 0.05$, compared to control; *t*-test. Data are represented as mean ± SEM.

Fig. S3. Saneyoshi et al.

A

```
Gallus gallus              DRSRPAMDTHASRMTQLKKQAALTGINGDVEGHG
Equus caballus             ERGRKTLDSHASRMTQLKKQAALSGINGGLESTS
Canis lupus familiaris     ERGRRALDSHASRMTQLKKQAALSGINGGLESPG
Mus musculus               ARGRRTLDSHASRMTQLKKQAALSGINGGLESAS
Homo sapiens               ERGRKTLDSHASRMAQLKKQAALSGINGGLESAS
Oryctolagus cuniculus      ERGRRTLDSHASRMAQLKKQAALSGGSGGLESAS
Anolis carolinensis        ERARYTGGTHVSRMAQLKKQAALPGINGGMEGNS
Xenopus tropicalis         TKVQNTMNTHASRMAQLKKQTAFSGMNGSIESNT
                            : : : .:*.***:*****:*: * .*.:*.
```

B

```
Tiam1      RTLDSHASRMAQLKKQAALSGIN
CaMKIIN1       KRPPKLGQIGRSKRVVIED
AIP                KKALRRQEAVDAL
```

C

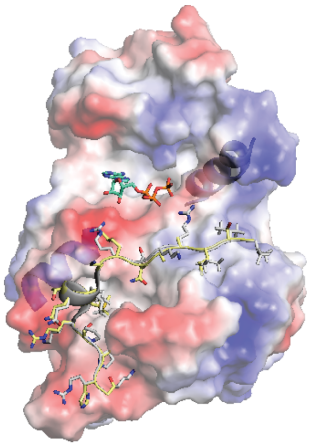

D

Tiam1 (predicted)

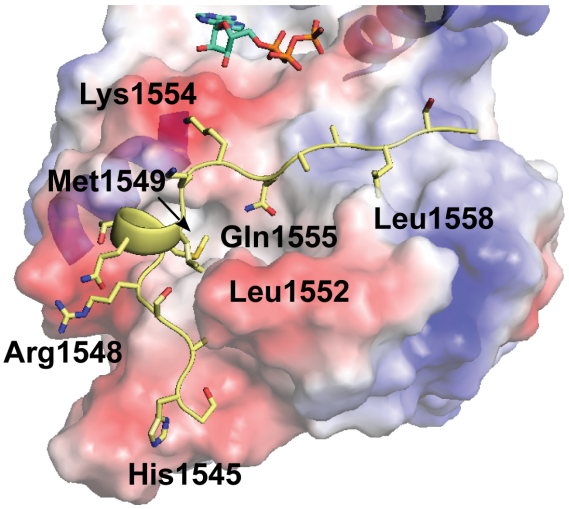

E

CaMKIIN1

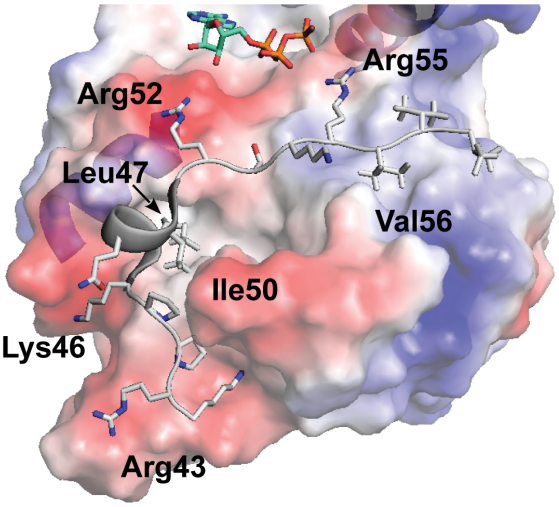

F

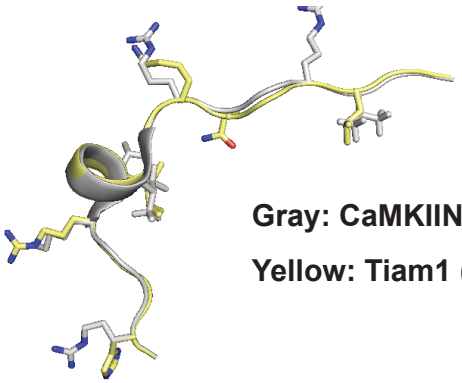

Gray: CaMKIIN1

Yellow: Tiam1 (predicted)

30

Figure S3, related to Figure 4. CBD of Tiam1 is conserved among vertebrate species, and a structural model of RAKEC formed between CaMKII and Tiam1.

A. Cross-species homology comparison of the CBD of Tiam1. Alignment was made by ClustalW program. The following information were used: *Gallus gallus*, XP_416699; *Equus cabllus*, XP_001498883, *Canis lupus familiaris*, XP_544855; *Mus musculus*, NM_009384.3; *Homo sapiens*, NM_003253.2; *Oryctolagus cuniculus*, XP_002716851; *Anolis carolinensis*, XP_003219107; *Xenopus Tropicalis*, XP_002938487.

B. A comparison of the CBD of Tiam1 and CaMKIIN1. The sequence in CaMKIIN1 important for binding, as determined by alanine scanning, is underlined (Coultrap and Bayer, 2011). Those residues that are particularly important are double-underlined. Consensus sequence (L/I)(K/R/H)(K/R)QXXΦ is in red and basic residues outside of the consensus sequence are in blue.

C-F. Prediction of binding between Tiam1 and CaMKII based on the X-ray crystallographic data of interaction between CaMKIIN1 and CaMKII (C) (Chao et al., 2010). Higher magnification of Tiam1/CaMKII interaction and the residues implicated in the binding are in D. CaMKIIN1/CaMKII interaction based on the original crystallographic data (E). Overlay of Tiam1 and CaMKIIN1 are shown (F).

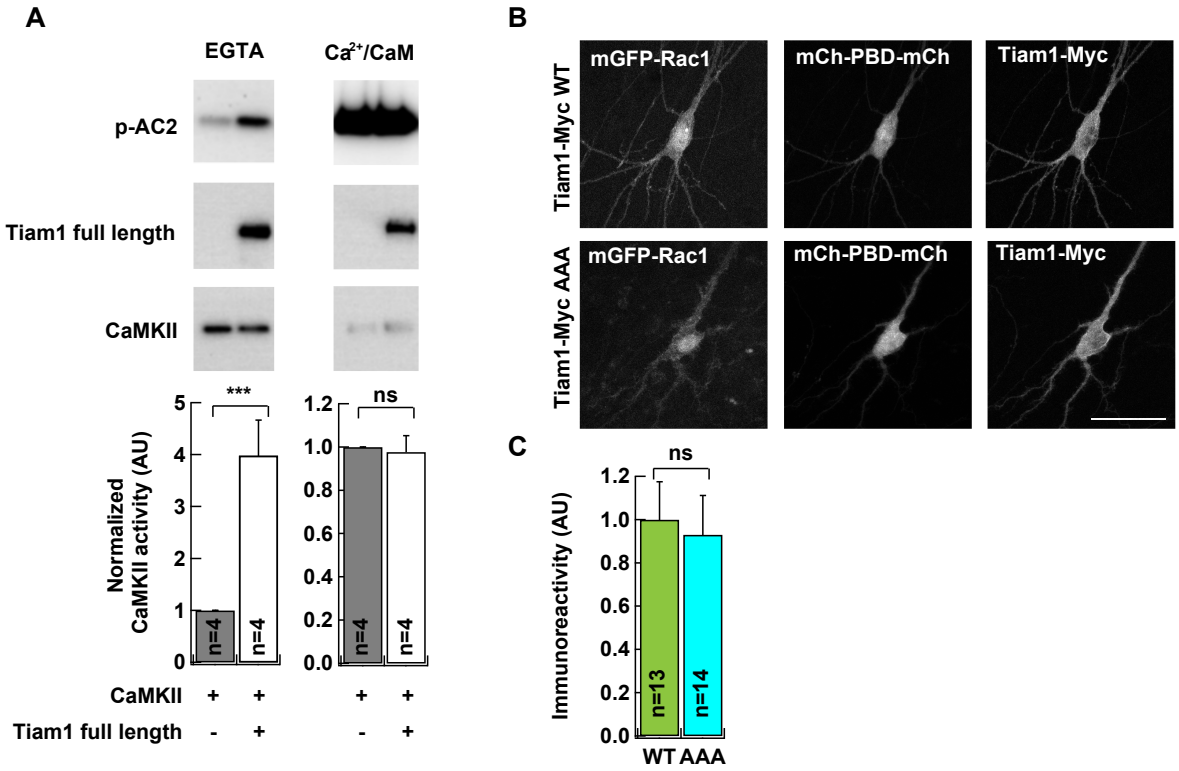

Figure S4, related to Figures 5 and 6. Binding with full length Tiam1 protein generates autonomous kinase activity of CaMKII and expression of WT and AAA Tiam1 rescue construct in neurons of hippocampal slice culture.

A. *In vitro* kinase assay of full length Tiam1-bound CaMKII using GST-AC2 as a substrate. CaMKII and Tiam1 were affinity-purified with a Flag antibody from HEK293T cells expressing Flag-tagged CaMKII or Tiam1. CaMKII was incubated with Tiam1 in the presence of Ca^{2+}/calmodulin to form a complex. Then EGTA was added to chelate Ca^{2+}. ATP was omitted in these steps to avoid autophosphorylation. Subsequently, the *in vitro* phosphorylation reaction was initiated by adding ATP in the absence (EGTA) or presence of Ca^{2+}/calmodulin (Ca^{2+}/CaM) using purified GST-AC2 as a substrate. The reaction products were subjected to western blotting with antibodies against phosphorylated-AKT substrate to detect phosphorylated AC2, Tiam1, and CaMKII. CaMKII bands in Ca^{2+}/CaM were shifted due to auto-

phosphorylation. Band intensities were measured and normalized to CaMKII without Tiam1 as one. ns, not significant; ***, $p < 0.01$, compared to CaMKII without Tiam1; *t*-test.

B. Representative images of neurons expressing shRNA against Tiam1, GFP-Rac1, mCherry-Pak1-mCherry, and shRNA resistant Tiam1 WT or AAA. Neurons in hippocampal organotypic slice culture were transfected with shRNA against Tiam1, GFP-Rac1, mCherry-Pak1-mCherry, and Myc-tagged shRNA resistant Tiam1 WT or AAA. Four days after transfection, slices were fixed, and stained with Myc antibody. Scale, 50 μm.

C. Quantification of Tiam1 rescue proteins in hippocampal organotypic slice culture. Immunoreactivities (IR) of Myc antibody were quantified in GFP and mCherry positive neurons. Relative IR was normalized to WT as one. ns, not significant; *t*-test.

Data are represented as mean ± SEM (A, C).

Fig. S5. Saneyoshi et al.

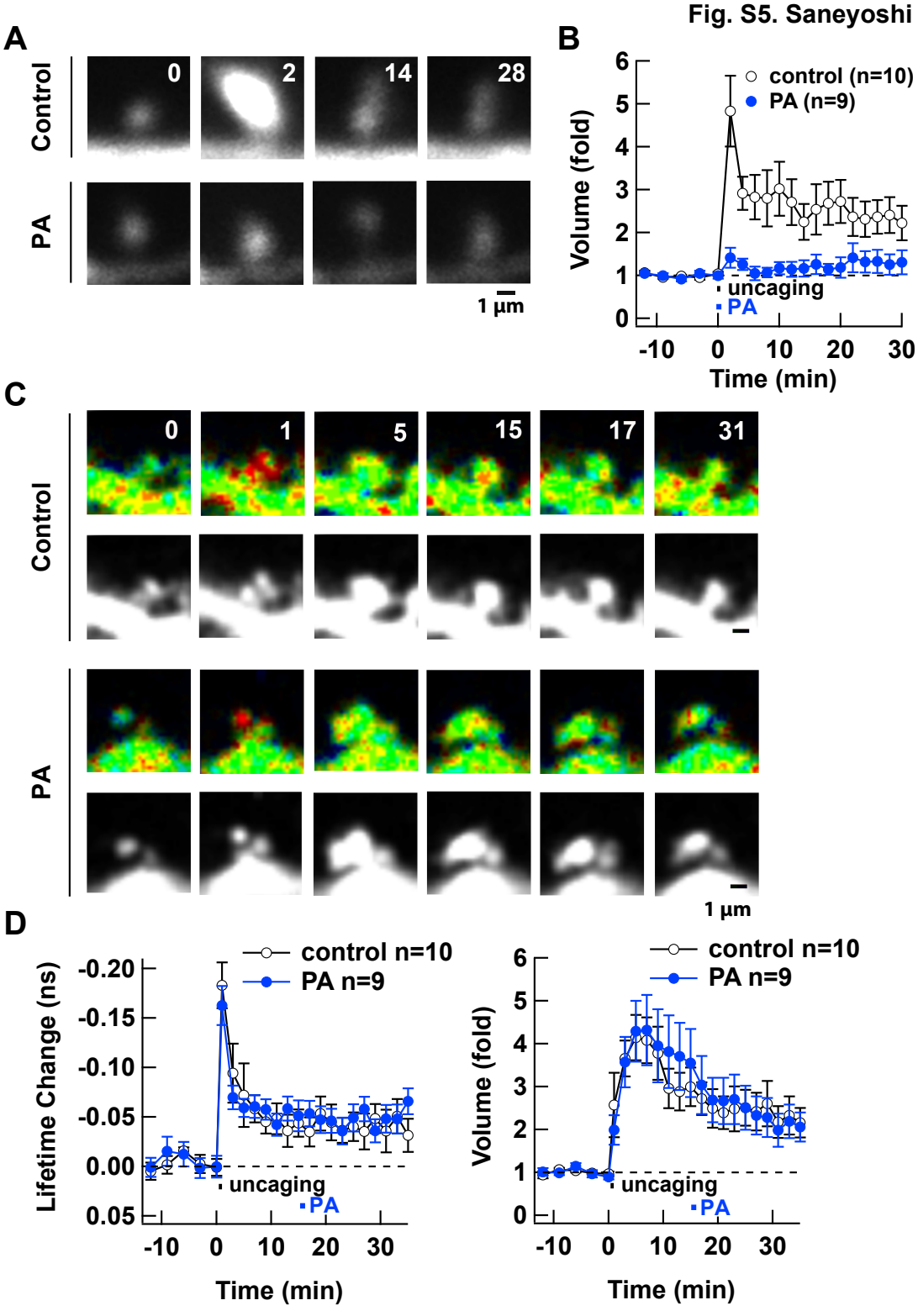

74

Figure S5, related to Figures 6. paAIP2 was not able to disrupt the Tiam1/CaMKII complex in stimulated spines

A. Sample images of sLTP in neurons in hippocampal organotypic slice culture coexpressing GFP and mCherry-paAIP2. Neurons were stimulated by uncaging of caged-glutamate using a 720 nm two-photon laser (uncaging, 2 ms pulses at 1 Hz for 30 sec) without or with simultaneous photoactivation (PA) of paAIP2 using 473 nm laser (200 ms pulses at 1 Hz for 1 min), which by itself does not cause uncaging of caged-glutamate (Matsuzaki et al., 2001). Control, without photoactivation; PA, with photoactivation.

B. Summary of the effect of photoactivation of paAIP2 at the same time with uncaging of glutamate. Spine volume was measured by fluorescent intensity of GFP.

C. Representative images of the interaction between Tiam1 and CaMKII with or without photoactivation of paAIP2 at 15 min after induction of sLTP. Warmer hues indicate more interaction. The distribution of Tiam1-GFP, as a proxy of structure, is shown (bottom).

D. Summary of FRET change (left) and volume (right) from multiple spines.

Data are represented as mean ± SEM (B, D).